TURUN YLIOPISTON JULKAISUJA
ANNALES UNIVERSITATIS TURKUENSIS

SARJA - SER. A I OSA - TOM. 382

ASTRONOMICA - CHEMICA - PHYSICA - MATHEMATICA

THE COSMIC PRODUCTION OF HELIUM

by

Luca Casagrande

TURUN YLIOPISTO
Turku 2008

From the Department of Physics
University of Turku
Turku, Finland

Supervised by

Dr. Chris Flynn and Dr. Laura Portinari
Tuorla Observatory
University of Turku
Turku, Finland

Reviewed by

Dr. Norbert Christlieb
Department of Astronomy and Space Physics
University of Uppsala
Uppsala, Sweden

and

Dr. Sofia Feltzing
Lund Observatory
University of Lund
Lund, Sweden

Opponent

Prof. Bengt Gustafsson
Department of Astronomy and Space Physics
University of Uppsala
Uppsala, Sweden

Cover picture: Luca Casagrande 2008

ISBN 978-951-29-3559-8 (PRINT)
ISBN 978-951-29-3560-4 (PDF)
ISSN 0082-7002
Painosalama Oy - Turku, Finland 2008

Fly me to the moon
And let me play among the stars
Let me see what spring is like
On Jupiter and Mars

From ’Fly Me to the Moon’ (Bart Howard, 1954)

Solution to the cover rebus in bibliography.

Acknowledgments

Many warm and well deserved thanks are due to all the people who contributed to make my life as a doctoral student so enjoyable over the last four years. These thanks are intended especially for the benefit of those who are actually not so interested in the rest of the thesis, but are driven to open these pages, or these three pages only, to know what I actually did during those years (or if their names are in the list!). To their convenience, I will sneak some informal tale from behind the scenes.

First, I would like to thank my supervisor, Christopher Flynn, for welcoming me to Tuorla, his scientific guidance and constant support throughout the entire thesis. He always made me feel comfortable and fully supported me even when I suffered from an embarrassing lack of scientific results and grants. Thanks to him, I attended various conferences and schools, worked in institutions abroad and networked with other researchers in the field. The month I spent in Mount Stromlo was not only highly productive but also very pleasant thanks to the company and the touristic guidance of Chris and Leena at various occasions. The student company at the house on the mountain was unique as well as were those cute wallabies jumping around when walking back from the observatory in the evening.

Laura Portinari joined Tuorla few months after my arrival and provided invaluable support to the thesis and helped to build my skills in the field of Galactic Chemical Evolution (work in progress, though). Her mid-afternoon genuine Italian espresso was an extraordinary chance to wake up my sleepy mind after the Majatalo lunch and also provided a moment for bright (from her side) scientific discussions on various topics of stellar astrophysics and chemical evolution, among others.

Chris & Laura significantly helped me by discussing, structuring and focusing the results obtained throughout these years. If I did not feel the famous mid-PhD crisis, it is certainly because of their support and optimism, too.

Leo Girardi: in addition to providing the theoretical stellar tracks computed especially for this thesis, he efficiently replied to all my questions on stellar modeling, as did Raul Jimenez thanks to whom I also had a great stay in Philadelphia. Even though I did not meet them personally, I wish to thank the co-authors of my last paper, Mike Bessell and Chris Koen for their help in that work. My former undergraduate advisor, Antonaldo Diaferio, helped me by keeping alive my interests in other exciting fields of astrophysics during my various visits in Turin. During these years, I also benefited from enlightening discussions with Johan Holmberg, Jorge Meléndez, Regner Trampedach, Daisuke Kawata, Sergio Sousa, Chris Thom and Hans Kjeldsen at many times. Even

though most of the time doing research is spent in front of a computer, I could share really nice moments and learn a lot from the various people I met at schools, conferences and visits abroad. This is also the place to note that my entire thesis would not exist as it is now if the formidable 2MASS data had not been publicly available!

I sincerely thank the whole Observatory staff and the other PhD students for an inspirational environment to do research and study, and in particular Janne–Dr. Alban for being one of my mentors in having fun and partying outside the working hours, not to forget Tuorla's Late Afternoon, starring Stefano Ciprini.

For financial support I have to thank the following contributors: Tuorla Observatory, the Finnish Graduate School of Space Physics and Astronomy, the Magnus Ehrnrooth foundation, the Otto A. Malm foundation, the Turku University Foundation and last but not least the Academy of Finland, through Chris and Laura. Special thanks also go to Leo Takalo for providing funds to attend the NOT summer school in La Palma. Observing with the NOT was NOT only highly instructive, but it turned out to be lots of fun inverting night and day as real astronomers do.

I thank the official reviewers of this thesis for speed reading and useful criticism. I am greatly honored that Prof. Bengt Gustafsson has agreed to act as my opponent in the public defense of this dissertation.

I had the fortune to come to Finland and find nice and friendly people here, from the very beginning, for which I have to thank Paula. Sami, Teemu & Jari soon turned from merely friendly flatmates to strict advisors to the Finnish lifestyle and properly educated me to ways of a tough guy from Pohjanmaa. I wonder if they fully succeeded (although I did my best!), but I really enjoyed their wit and relaxed style. By the Galilean concept of clear evidence of sense, they indisputably proved that it is also a lot of fun inverting night and day as non–astronomers do! Along the same lines, I am glad to shortlist Osmo, Ville, Mikko, Jojo, Kimmo, Annastiina, Peter & Tero.

My Finnish language skills have remained at a steady level throughout these years and it is still a matter of debate whether they will end up in the big crunch or not. I could not cope with the many issues (well, except for understanding yet another parking fine) concerning everyday life without the help of the ihanat people around me. I have been truly blessed in this respect. I have only good memories of my time in Finland, and I have to thank Sini for that.

Of course, as a migrant, I had the secret dream of becoming a godfather: I probably misunderstand something, but I am the happiest person ever to have Giorgia and Feliks as my godchildren. Although most of the time was actually spent in Finland, the Italian connection has always been strong. That was certainly because of the good company of Giacomo, Giulio & Ruggero, besides the other members of Samba Carioca School the few occasions I got time to play there.

The love with my hometown grew stronger at every return (and every New Year's Eve) thanks to the incredible and trustful group of friends I will always count on (e anche di più!): Alberto, Alessia, Anna, Asso, Bruna, Daniele, Elisa1, Elisa2, Fabio, Filippo, Giorgio, Nadia, Paolo, Pietchro and Silvana. To those involved in this business,

I already promise my attendance to the next 10–year–meeting, to be held in Mondovì in April 2017 (Indiscutibilmente Posso Prometterlo Ora), but I look forward to closer events to enjoy with you!

My interest toward astronomy started when I was just a few years old, from the wonder of looking at the sky from my family's summer house and the fear of learning from my brother that stars are actually much much bigger than the Earth! Everything started there and then and I consider that as the first proof of support by my family towards my passion, support that has never been lacking. Ringrazio pertanto i miei genitori per l'affetto e l'appoggio nelle mie scelte. Senza di loro non sarei arrivato fino a qui.

Finally, to those who wish to know the tips and tricks of accomplishing a PhD, I confidently say that all the people mentioned here are part of it and to them I owe my deepest gratitude.
Kiitos!

Luca Casagrande

Contents

List of publications

I *Accurate fundamental parameters for lower main–sequence stars*
Casagrande L., Portinari L. and Flynn C.
MNRAS **373**, 13 (2006)

II *The helium abundance and $\Delta Y/\Delta Z$ in lower main–sequence stars*
Casagrande L., Flynn C., Portinari L., Girardi L. and Jimenez R.
MNRAS **382**, 1516 (2007)

III *M dwarfs: effective temperatures, radii and metallicities*
Casagrande L., Flynn C., Bessell M. and Koen C.
submitted to MNRAS

CHAPTER 1
Introduction

Low mass stars are long–lived objects and can be regarded as snapshots of the stellar populations formed at different times over the history of our Galaxy, the Milky Way. Not only these stars retain in their atmospheres a fossil record of the chemical elements in the interstellar medium at the time of their formation, but also their orbits similarly encode their dynamical histories. In this thesis we deal with the first of these two aspects. We characterize the physical and chemical properties of low mass stars in the more general framework of Galactic Chemical Evolution, with a particular attention to the helium production.

Traditionally, F and G dwarfs have been preferential targets for studies dealing with various aspects of the chemical evolution of the Milky Way (e.g. Wallerstein 1962; Pagel & Patchett 1975; Edvardsson et al. 1993; Wyse & Gilmore 1995; Feltzing, Holmberg & Hurley 2001; Bensby, Feltzing & Lundström 2003; Nordström et al. 2004; Brewer & Carney 2006). However, F and G dwarfs are sufficiently massive that some of them have begun to evolve away from the main-sequence and these evolutionary corrections might complicate the comparison with chemical and stellar evolutionary models.

It has been long recognized that K dwarfs make a cleaner sample because for these stars the evolutionary corrections are negligible. K dwarfs are intrinsically fainter than stars of earlier spectral type, so it has not been until recently that high-quality spectra and accurate abundance analyses have become common (e.g. Feltzing & Gustafsson 1998; Allende Prieto et al. 2004). To fully understand the information carried by these stars, accurate stellar parameters and most notably effective temperatures, are needed. The determination of effective temperatures and bolometric luminosities for a local sample of K and G dwarfs has been subject of Paper I of this thesis.

With the availability of better data, K dwarfs have begun to be used for chemical evolution studies (e.g. Kotoneva et al. 2002). K dwarfs display a similar metallicity distribution as G dwarfs (e.g. Flynn & Morell 1997), in which most stars have metallicities around and slightly below the solar value, a feature not expected in the simplest models of Galactic Chemical Evolution (i.e. the “G dwarf problem”). Although nowadays the abundance patterns of metals in K dwarfs is relatively straightforward to measure, the same cannot yet be said for M dwarfs. Recently, major improvements in model atmospheres of very cool stars and the availability of high-quality infrared data have boosted a number of studies on the subject. Taking advantage of such a favourable conjunction, the determination of precise physical parameters for M dwarfs has been tackled on Paper III. The study of very cool dwarfs seems to confirm also the existence of an “M dwarf

problem", but further studies are needed (Bonfils et al. 2005). The definition of an accurate and homogeneous effective temperature scale for G-K-M dwarfs as well as the technique presented in Paper III for estimating M dwarf metallicities will be major steps in this direction.

The work presented in Paper I and III is crucial to precisely determine the location of low mass stars in the HR diagram. With such an accuracy it is possible to address various questions related to the fine structure of the lower main-sequence, which has relevance for both chemical evolution and stellar astrophysics, as discussed in Paper II and III.

Presently, G and K dwarfs are the stellar populations most used for Galactic Chemical Evolution studies, since their metal abundance pattern provides valuable information for disentangling the complex puzzle of the Milky Way's formation. Parallel to the metal content in a stellar population, also the helium abundance and the differential production rate of the helium mass fraction Y relative to the metal mass fraction Z (i.e. $\Delta Y/\Delta Z$) has profound implications in many areas of astrophysics and cosmology.

The ratio can be used to infer the primordial helium abundance Y_P by extrapolating to $Z = 0$. This technique is usually applied to extragalactic HII regions as discussed in Chapter 2, where the primordial helium abundance predicted in the standard Big Bang Nucleosynthesis scenario is also outlined.

The ratio $\Delta Y/\Delta Z$ also governs the stellar clock and thus how long stars live. The position of not evolved dwarf stars (i.e. those with mass approximately below $0.8\,M_{\odot}$) on the HR diagram is also uniquely (or almost) determined by their helium and metal content. The ratio $\Delta Y/\Delta Z$ thus determines the broadening of the lower main-sequence and it can be understood in simplified terms by means of so-called quasi-homology relations. This is explained in Chapter 3, where quasi-homology stellar models are introduced to provide the theoretical background behind the measurement of $\Delta Y/\Delta Z$, which is then the subject of Paper II.

Starting from its primordial abundance, helium is mildly topped up by stars, together with the production/destruction of other elements. Whereas metals mainly come from supernovae with high mass progenitors, helium is also ejected into the interstellar medium by mass loss from intermediate and low mass stars: $\Delta Y/\Delta Z$ can thus be computed from stellar evolutionary theory for a given initial mass function. This is discussed in Chapter 4 where a chemical evolution model for the Solar Neighbourhood is also presented. The ratio $\Delta Y/\Delta Z$ predicted by the chemical evolution model is used to validate the extrapolation technique presented in Chapter 2 and to discuss the results obtained in Paper II.

Finally in Chapter 5 the results obtained throughout the thesis are summarized. Future prospects for projects arising from the current work are also briefly outlined.

CHAPTER 2
Big Bang Nucleosynthesis

"...this big bang idea ..."

Fred Hoyle on March 28, 1949 – BBC Third Programme

2.1 Historical perspective

The idea of primordial nucleosynthesis dates back to Gamow (1946) and the Big Bang theory of the Universe pioneered by Gamow, Alpher and Herman in the late 1940s and early 1950s. One of the first steps in this direction was made in the "$\alpha\beta\gamma$" paper by Alpher, Bethe & Gamow[1] (1948): they supposed that during the first few minutes of the radiation–dominated Universe, matter was originally present in form of neutrons and that, after some free decay, protons captured neutrons and successive captures built up all the elements.

Hayashi first put the theory on a sound physical basis by pointing out that, at the high densities and temperatures involved, there would be thermal equilibrium between protons and neutrons at first, followed by a freeze–out, and this intensified the difficulties already inherent in that theory that the absence of stable nuclei at mass number 5 and 8 would prevent significant nucleosynthesis beyond helium. In the meantime, progress in the theory of stellar evolution and nucleosynthesis led to comparative neglect of the Big Bang Nucleosynthesis (BBN) theory, until the detection of the cosmic microwave background (CMB) radiation (Penzias & Wilson 1965). The existence of the CMB had been foreseen already by Gamow and proposed on a more solid base by Dicke et al. (1965) in the Big Bang framework.

The discovery of the CMB marked a major step in favour of the BBN theory, which was developed subsequently by Peebles, Wagoner, Fowler, Hoyle, Schramm, Steigman and others. Such a theory intermingles cosmology and particle physics and it has been very successful in several respects, as we discuss in more details throughout this Chapter.

2.2 Primordial abundances: a brief overview

As the Universe evolved from its early, hot, dense beginnings to its present, cold, dilute state, it passed through a brief epoch when the temperature and density of its nucleon

[1] Although Bethe did not take part to this work his name was included by Gamow to complete the "$\alpha\gamma$" sequence.

component were such that nuclear reactions building complex nuclei could occur. It is worthwhile to point out here that throughout the thesis, unless stated, although we talk about hydrogen (H), deuterium (D), tritium (t), helium (^{4}He) and more complex elements, we always refer to nuclei.

The nuclear reactions occurring in the early Universe are different from those occurring in stars in several ways: the cosmological density is dominated by radiation, and the matter density is much lower than in stars. More rigorously, at temperatures[2] much higher than 1 MeV the Universe is filled with radiation (photons, $e^{\pm}$, neutrinos of all flavors) along with baryons (nucleons) and dark matter particles. Nuclear and weak reactions are occurring among the neutrons, protons, $e^{\pm}$ and neutrinos at rates fast compared to the Universe expansion rate. The balance between neutrons and protons is maintained by the weak interactions[3]

$$n \longleftrightarrow p + e^- + \overline{\nu}_e \tag{2.1}$$

$$\nu_e + n \longleftrightarrow p + e^- \tag{2.2}$$

$$e^+ + n \longleftrightarrow p + \overline{\nu}_e. \tag{2.3}$$

For temperatures of few tens of MeV, protons and neutrons are not relativistic (i.e. $k_B T \ll m_p c^2 \sim m_n c^2$) and their equilibrium —in the standard scenario without asymmetry between the number of ν_e and $\overline{\nu}_e$— can be described by the Maxwell–Boltzmann distribution. Defining N_n (N_p) as the number density of neutrons (protons), the neutron–to–proton ratio is

$$\left(\frac{N_n}{N_p}\right) \sim \exp(-Q/k_B T) \tag{2.4}$$

where $Q = (m_n - m_p)c^2 = 1.293$ MeV. When the Universe is hot enough, i.e. for $k_B T \gg Q$ the ratio given by equation (2.4) is almost one and the number of protons and neutrons in the Universe practically identical.

While neutrons and protons are interconverting, they are also colliding among themselves creating complex nuclides as deuterium $n + p \longleftrightarrow \mathrm{D} + \gamma$. However, at early times, when the density and the average energy of the photons are very high, the newly formed deuterium is bathed in a background of high–energy gamma rays capable of photodissociating it. Therefore, deuterium is photodissociated before it can capture a neutron, a proton or another deuterium to build heavier nuclei. This *bottleneck* to BBN persists until the temperature drops sufficiently below the binding energy of deuterium at about 2.2 MeV. As the Universe expands and cools, the lighter protons are favoured over the heavier neutrons and the neutron–to–proton ratio decreases, tracking the equilibrium form in equation (2.4). However, if the equilibrium is to be maintained, the ratio would

[2] In the rest of the Chapter we talk of temperature in terms of energy, where $1\mathrm{MeV} \sim 1.2\ 10^{10}$ K.

[3] The reaction (2.1) is the least important for the equilibrium because of the long lifetime of the neutron, $\tau_n = 885.7 \pm 0.8$ s (Yao et al. 2006) as compared to the Hubble time of the primordial Universe. The backward reaction is also less likely to occur as it involves a three body process.

decrease to a very small value at low temperature. The neutron–to–proton ratio therefore freezes–out at some characteristic value. As the temperature of the Universe decreases, other processes occur too. At about 1 MeV, neutrinos decouple since they are no longer energetic enough for $\nu\overline{\nu} \longrightarrow e^- e^+$ to happen. Immediately following the neutrino decoupling, $e^+e^- \longrightarrow 2\gamma$ is possible, but not the reverse. As the $e^\pm$ pairs annihilate, they transfer their entropy to the photons alone, thereby raising the photon temperature relative to that of the neutrinos. Following the annihilation of the positrons and electrons, a large number of photons remains. From now on, as the Universe expands, the densities of baryons and photons in a comoving volume are unchanged with time. It is thus useful, and conventional, to quantify the universal abundance of baryons by comparing the number density of baryons (n_B) to the number density of CMB photons (n_γ)

$$\eta_{10} = 10^{10}\eta_B \equiv 10^{10}(n_B/n_\gamma) \tag{2.5}$$

where η_{10} measured at BBN, at recombination and at present remains the same for the reason outlined above (e.g. Steigman 2007).

By this time, when the energy of the Universe is somewhat below 1 MeV, the reactions (2.2) and (2.3) cease and the neutron–to–photon ratio is given approximately by its equilibrium value

$$\left(\frac{N_n}{N_p}\right)_{\rm freeze-out} \sim \exp(-Q/k_B T) \sim \frac{1}{6}. \tag{2.6}$$

After the freeze–out, the neutron–to–proton ratio does not remain truly constant, but actually slowly decreases due to occasional weak interactions, eventually dominated by free neutron decays (2.1). Unless the neutrons are not locked away in nuclei before $\sim \tau_n$, their relic abundance would decay to zero. Since the freeze–out point (2.6) occurs at an age of the Universe of few seconds, there are only a few *e*-foldings of expansion available to save the neutrons.

The baryon–to–photon ratio η_{10} sets the energy at which the photodissociation of deuterium becomes inefficient, which is at about 0.1 MeV. Before having time to decay, most of the neutrons end up in ^{4}He nuclei through the following set of reactions

$$\begin{aligned}
p + n &\longrightarrow \mathrm{D} + \gamma \\
\mathrm{D} + \mathrm{p} &\longrightarrow {}^3\mathrm{He} + \gamma \\
\mathrm{D} + \mathrm{D} &\longrightarrow {}^3\mathrm{He} + n \\
\mathrm{D} + \mathrm{D} &\longrightarrow p + \mathrm{t} \\
{}^3\mathrm{He} + n &\longrightarrow p + \mathrm{t} \\
\mathrm{t} + \mathrm{D} &\longrightarrow {}^4\mathrm{He} + n \\
{}^3\mathrm{He} + \mathrm{D} &\longrightarrow {}^4\mathrm{He} + p
\end{aligned} \tag{2.7}$$

while the ratio (2.6) actually decreases to $\sim 1/7$ (e.g. Kolb & Turner 1990).

It is clear from the above reactions that in the early Universe, the only nuclei produced in any significant abundance are H and $^4\mathrm{He}$. The latter because it is the most stable light nucleus (i.e. that with the highest binding energy), and the former because there are not enough neutrons for all the protons to bind with, and so some protons are left over. We can easily get an estimate of their relative abundance, normally quoted as the mass fraction. Since every helium nucleus contains two neutrons, all neutrons end up in helium and the *number* density of $^4\mathrm{He}$ is $N_{\mathrm{He}} = N_n/2$. Each $^4\mathrm{He}$ nucleus weights about four proton masses, so the primordial fraction of the total *mass* in helium, known as Y_P is[4]

$$Y_P = \frac{4N_{\mathrm{He}}}{N_{\mathrm{tot}}} = \frac{2N_n}{N_n + N_p} \sim 0.25. \tag{2.8}$$

This simple treatment tells us that the fraction of matter in the Universe that ends up into helium is about 25% of the total. A more rigorous and detailed treatment involves keeping track of the whole network of nuclear reactions rates and the expansion of the Universe. However, the conclusion remains that about 25% of the Universe's primordial composition is in helium, with all the rest in hydrogen. For this reason, it is a common habit among astronomers to talk of hydrogen mass fraction X, helium mass fraction Y and metal mass fraction Z, where "metal" is to be understood as all elements heavier than helium. The condition $X + Y + Z = 1$ obviously holds.

The full BBN reaction network is considerably more complicated (e.g. Wagoner 1973; Kawano 1992) but allows one to estimate the trace abundances of all the other nuclei which form in the early Universe. The main reactions occurring during BBN, in addition to those in (2.7), are

$$\begin{aligned} {}^3\mathrm{He} + {}^4\mathrm{He} &\longrightarrow {}^7\mathrm{Be} + \gamma \\ \mathrm{t} + {}^4\mathrm{He} &\longrightarrow {}^7\mathrm{Li} + \gamma \\ {}^7\mathrm{Be} + n &\longrightarrow {}^7\mathrm{Li} + p \\ {}^7\mathrm{Li} + p &\longrightarrow {}^4\mathrm{He} + {}^4\mathrm{He} \end{aligned} \tag{2.9}$$

and they are all shown in Figure 2.1.

By the time $^4\mathrm{He}$ is produced, Coulomb–barrier suppression is very significant. This fact, together with the absence of tightly–bound isotopes with mass 5 and 8, prevented significant nucleosynthesis beyond $^4\mathrm{He}$. The few reactions that manage to bridge the mass 5 gap lead mainly to mass 7, producing $^7\mathrm{Li}$ and $^7\mathrm{Be}$. Later, when the Universe has cooled further, $^7\mathrm{Be}$ captures an electron and decays to $^7\mathrm{Li}$. For the range of η_{10} of interest, the BBN predicted abundance of $^6\mathrm{Li}$ is more than 3 orders of magnitude below that of the more tightly bound $^7\mathrm{Li}$. Finally the other gap at mass 8 ensures that there is no significant production of heavier nuclides, which are in fact produced in stars. It

[4]Defined this way, Y_P is not really the mass fraction because this expression adopts precisely 4 for the $^4\mathrm{He}$ to H mass ratio. However, the reader should be warned that Y_P defined this way is conventionally referred to by cosmologist as the $^4\mathrm{He}$ mass fraction (e.g. Steigman 2007)

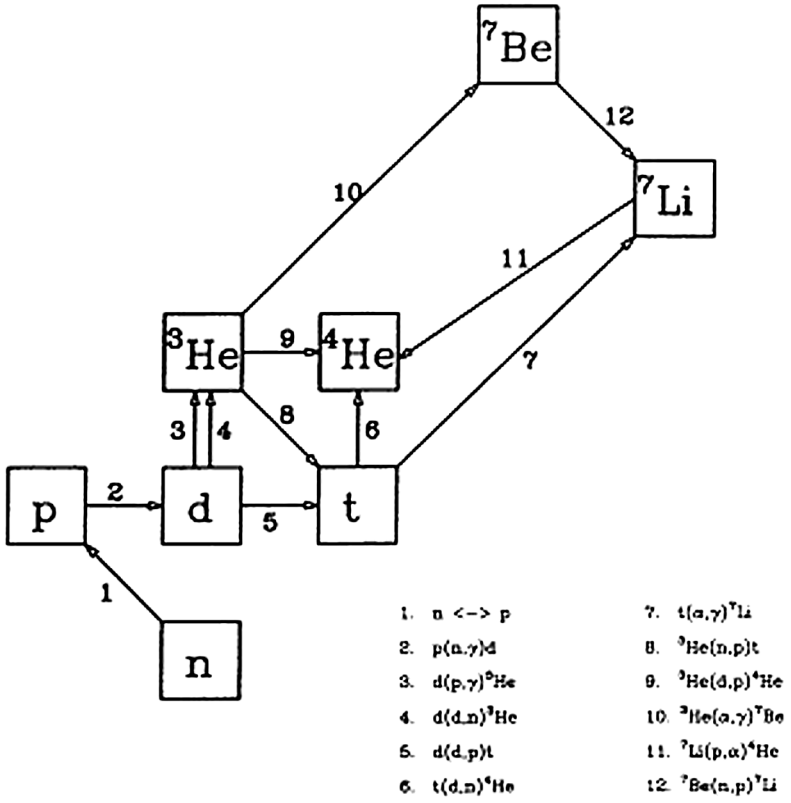

Figure 2.1: *Network diagram of the 12 primary reactions in the processing of the light elements. The nucleus of deuterium is indicated by d (from Smith, Kawano & Malaney 1993).*

is therefore a very good approximation to assume that the primordial mass fraction of metal is $Z = 0$.

The primordial nuclear reactor is thus short-lived. As the temperature drops below $\sim$ 30 keV, when the Universe is about 20 minutes old, Coulomb barriers abruptly suppress all nuclear reactions. Afterwards, until the first stars form, no pre–existing, primordial nuclides are destroyed, except for those like t and ^{7}Be that are unstable and decay to ^{3}He and ^{7}Li respectively, and no new nuclides are created (e.g. Iocco et al. 2007). In these 20 minutes the BBN has run its course.

2.3 Beyond the standard model

In the previous Section we have presented the standard BBN scenario. Here we briefly mention possible departures from such a picture and illustrate how in this case the pre-

dicted abundances depend on additional parameters. The reader can refer e.g. to Kneller & Steigman (2004) for further details.

The Hubble parameter, H measures the expansion rate of the Universe. Deviations from the standard model (H') may be parametrized by an expansion rate parameter $S \equiv H'/H$ or equally by the equivalent number of neutrinos $\Delta N_\nu \equiv N_\nu - 3$. ΔN_ν and S are equivalent ways to quantify any deviation from the standard model expansion rate and ΔN_ν is not necessarily related to extra or fewer neutrinos. Changes (from the standard model) in the expansion rate at BBN would modify the neutron abundance and the time available for nuclear production/destruction, changing the BBN predicted relic abundances. For example, in the case of ^{4}He, a faster expansion would provide less time for neutrons to transform into protons, and the higher neutron fraction would result in an increase of Y_P. The primordial mass fraction of ^{4}He is thus an excellent chronometer of the early Universe expansion rate.

In the currently most popular particle physics models the universal lepton and baryon asymmetries are comparable, so as to keep the Universe globally neutral. Because any charged lepton asymmetry is limited by the baryon asymmetry to be very small, any further non–negligible lepton asymmetry must be among the neutral lepton, the neutrinos. Neutrino asymmetries orders of magnitude larger than the baryon asymmetry are in fact not excluded by any experimental data. Such neutrino asymmetries are quantified by the parameter ξ_α ($\alpha \equiv e, \mu, \tau$). Although any neutrino asymmetry increases the energy density in the neutrinos, resulting in an effective $\Delta N_\nu > 0$, the range of ξ_α of interest to BBN is limited to sufficiently small values that the increase in S due to a non–zero ξ_α is negligible. However, a small asymmetry between electron type of neutrinos and antineutrinos, can have a significant impact on BBN since ν_e affects the interconversion of neutrons to protons. Thus, a non–zero ξ_e results in different numbers of ν_e and $\overline{\nu}_e$, altering the neutron–to–proton ratio at BBN, therefore changing the yields of the light nuclides. For example, in the case $\xi_e > 0$, the neutron–to–proton ratio increases over its standard BBN value, leading to an increase in the ^{4}He yield.

Any model beyond the standard BBN can therefore be parametrized essentially as function of S and ξ_e. High accuracy measurements of primordial abundances have thus the possibility to constrain and/or open interesting windows on the physics and the cosmology beyond the standard models. We illustrate and briefly discuss some of the most recent measurements of light elements in the next Section. As regards helium, such alternative models predict variations in its primordial abundance up to a percent or less and therefore do not provide any viable solution to the low helium abundances presented in Paper II, which are most likely entirely stemming from inadequacies in extant low mass, low–metallicity stellar models.

2.4 Predicted and observed abundances

Over the years, many researchers have written computer codes to integrate the coupled set of differential equations that track element production/destruction to solve for the BBN predicted abundances of the light nuclides.

In the standard BBN scenario with $S = 1$ ($N_\nu = 3$) and $\xi_e = 0$ the predicted primordial abundances depend on only one free parameter, the baryon density η_{10} as shown in Figure 2.2. Simple arguments help us to understand this. The reactions burning D, t and ^{3}He to ^{4}He are fast compared to the early Universe expansion rate, ensuring that almost all neutrons present at the time are incorporated into ^{4}He once the deuterium bottleneck is breached. As a result, the ^{4}He primordial abundance is very insensitive to the baryon abundance. The very slight increase in Y_P with increasing η_{10} reflects the fact that for a higher baryon density BBN begins slightly earlier, when slightly more neutrons are available. Nuclear reactions burn D, t and ^{3}He to ^{4}He at a rate which increases with increasing nucleon density, accounting for the decrease in the abundances of D and ^{3}He (the latter receives a contribution from the β-decay of t) with higher values of η_{10} (e.g. Steigman 2007).

The behaviour of ^{7}Li reflects the two pathways to mass 7. At relatively low values of η_{10}, mass 7 is largely synthesized in form of ^{7}Li by $\mathrm{t}(\alpha,\gamma)^7\mathrm{Li}$ reactions. As η_{10} increases ^{7}Li is destroyed more efficiently by collisions with protons. Further increasing η_{10}, mass 7 is largely synthesized as ^{7}Be via $^3\mathrm{He}(\alpha,\gamma)^7\mathrm{Be}$ reactions. The end product of this channel, ^{7}Be is more tightly bound than ^{7}Li and, therefore harder to destroy. Therefore, as η_{10} increases the primordial abundance of ^{7}Be increases. Later when the Universe cools and neutral atoms begin to form, ^{7}Be captures an electron and β-decays to ^{7}Li. These two paths to mass 7 account for the valley shape of the ^{7}Li abundance curve in Figure 2.2.

The success of BBN relies on its ability to predict the observed primordial abundances and, conversely, to learn about the cosmological parameters using the same abundances. Now that observations of the CMB and of the distribution of the Large Scale Structure (LSS) have become sufficiently precise, the range of η_{10} of interest is restricted to around $5.7 < \eta_{10} < 6.5$ (Spergel et al. 2007; Tegmark et al. 2004). Assuming standard BBN, it is therefore possible to find accurate linear fits to the predicted abundances as function of η_{10} only

$$y_D \equiv 10^5(\mathrm{D/H}) = 2.68(1 \pm 0.03)(6/\eta_{10})^{1.6} \tag{2.10}$$

$$y_3 \equiv 10^5(^3\mathrm{He/H}) = 1.06(1 \pm 0.03)(6/\eta_{10})^{0.6} \tag{2.11}$$

$$Y_P = 0.2483 \pm 0.0005 + 0.0016(\eta_{10} - 6) \tag{2.12}$$

$$y_{\mathrm{Li}} \equiv 10^{10}(^7\mathrm{Li/H}) = 4.30(1 \pm 0.1)(\eta_{10}/6)^2. \tag{2.13}$$

The comparison of predictions and observations is far from trivial because of the further processing of the nuclei since the end of BBN. Deuterium is the baryometer of choice,

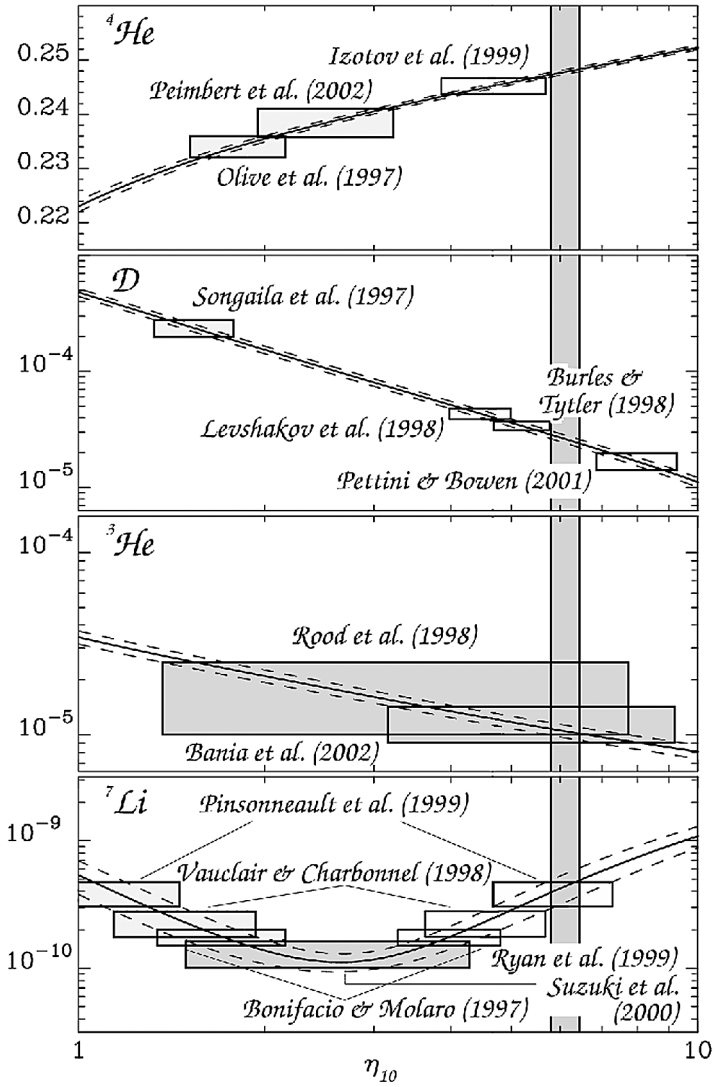

Figure 2.2: *Solid lines: primordial abundances of* ^{4}He *(mass fraction),* D, ^{3}He *and* ^{7}Li *(number ratios relative to hydrogen) as a function of* η_{10} *assuming standard BBN. The dashed lines are* 1σ *deviations. Some of the observations discussed throughout this chapter are shown with* 1σ *boxes. The vertical band represent the WMAP* η_{10} *range (from Romano et al. 2003).*

because of the strong dependence of its abundance on η_{10} and because BBN observed abundance should have only decreased as gas is cycled through stars where deuterium is burned to heavier, more tightly bound nuclei. As a result, deuterium observed anywhere in the Universe, at any time during its evolution, should provide a lower bound to its primordial abundance (e.g. Pettini 2006). Further, the deuterium observed in the

high redshift, low metallicity QSO absorption line systems should be very nearly primordial, although hydrogen absorption in a cloud along the same line of sight can bias measurements toward a much higher deuterium abundance (e.g. Steigman 1994). Although the data is still scarce and the scatter remains large, the measurements appear to converge to a mean primordial value $y_D \sim 2.4 \pm 0.4$ (e.g. Burles & Tytler 1998; Pettini & Bowen 2001; O'Meara et al. 2001, 2006) which corresponds (Eq. 2.10) to $\eta_{10} \sim 6.4$, in excellent agreement with the value $\eta_{10} = 6.116$ obtained from WMAP (Spergel et al. 2007). In contrast, the post-BBN evolution of ^{3}He and of ^{7}Li are considerably more complicated, involving the competition between production, destruction and survival. As a result, at least so far, the current, locally observed (in the Galaxy) abundances of these nuclides have been considered of less value than that of deuterium. Indeed, for the currently accepted range of η_{10}, the primordial abundance of ^{3}He is predicted to lie in the narrow range $1.0 < y_3 < 1.1$, in excellent agreement with that inferred from Galactic observations of distant, metal–poor HII regions (Bania, Rood & Balser 2002). Thus, ^{3}He provides similar, but less compelling constraints than does deuterium. In the post BBN Universe, ^{7}Li along with ^{6}Li, ^{9}Be, ^{10}B and ^{11}B, is produced in the Galaxy by cosmic ray spallation/fusion reactions (e.g. Pagel 1997). Furthermore, observations of super–lithium–rich red giants provide evidence that at least some stars are net producers of lithium (e.g. Brown et al. 1989; de la Reza 2000). Therefore, in order to probe the BBN yield of ^{7}Li, it is necessary to restrict attention to the oldest, most metal–poor halo stars in the Galaxy. The ^{7}Li abundance measured in the atmosphere of old stars is a factor of two to four lower than the predicted abundance assuming the currently accepted value of η_{10} (Spite & Spite 1982; Ryan, Norris & Beers 1999; Asplund et al. 2006; Bonifacio et al. 2007) although, most notably, the adopted temperature scale (e.g. Meléndez & Ramírez 2004) and the effect of diffusion (e.g. Korn et al. 2006, 2007) could help in solving the discrepancy.

Although the main focus of the present thesis has been the study of helium, some of the results obtained might be of relevance for the determination of other primordial abundances. The derivation of an accurate effective temperature scale for G-K-M dwarfs is subject of Paper I and III and the effect of diffusion in altering the position of dwarf stars in the HR diagram is also briefly discussed in Paper II. The extension of the temperature scale presented in Paper I and III to very metal–poor and earlier spectral type stars will be valuable for accurate measurements of the primordial lithium abundance in such a type of stars.

2.4.1 Helium

As gas cycles through generations of stars, hydrogen is burned to ^{4}He and beyond, increasing the helium abundance above its primordial value Y_P (Burbidge, Burbidge, Fowler, Hoyle 1957). As a result, the ^{4}He mass fraction in the Universe at any given epoch after the Big Bang, Y, contains a contribution from stellar nucleosynthesis, so that $Y > Y_P$.

Helium abundances can be estimated in various objects with different techniques, but direct measurements are still rather challenging. Measurements from the Voyager and Galileo spacecraft data on Jupiter and Saturn have returned a helium mass fraction in the range $0.19 - 0.25$ (Conrath & Gautier 2000). The value for the interior of the Sun is based on theoretical models of its evolution, constrained by its known mass, age, chemical composition (apart from helium itself!) and present day luminosity and radius (Chapter 3 and Paper II). Helioseismology has led to greatly improved understanding of the Sun's internal structure and it also indicates an appreciably lower helium abundance in the convective envelope, which is attributed to gravitational settling (e.g. Christensen-Dalsgaard, Proffitt & Thompson 1993; Basu, Pinsonneault & Bahcall 2000). Based on seismic data, the helium abundance in the solar convective envelope is estimated to range from $Y_{\rm surf,\odot} = 0.24$ to $Y_{\rm surf,\odot} = 0.25$ (see Basu & Antia 2008 for a review) whereas the standard solar model predict $Y_\odot = 0.2725$ and $Y_\odot = 0.2600$ if the Grevesse & Sauval (1998) or the Asplund, Grevesse & Sauval (2005) heavy element abundances are used (Bahcall, Serenelli & Basu 2006). Estimates of helium in the chromosphere have been made on the basis of hydrogen and helium emission lines from prominences, but these measurements are quite imprecise[5]. What it is important from the above discussion is that most of the helium in the Sun has primordial origin and its exact value has been increased with respect to Y_P only by few hundreds. The most metal–poor stars in the solar neighbourhood are thus of particular interest, because their content of heavy elements is so low that they can be considered to have been born with essentially the primordial helium abundance. The attempt to determine the helium abundance in the most metal–poor, non evolved dwarf stars in the Solar Neighbourhood is the subject of Paper II.

Accurate measurements of helium abundances come from measurements of recombination lines of hydrogen and helium in the emission spectra of planetary nebulae (e.g. Pottasch, Bernard-Salas & Roellig 2007) and HII regions (e.g. Izotov, Thuan & Stasińska 2007; Peimbert, Luridiana & Peimbert 2007), using theoretical effective recombination coefficients calculated from quantum mechanics. In Galactic HII regions it is also possible to observe radio recombination lines, which is especially useful when the optical spectrum is obscured by dust (e.g. Balser 2006). Peimbert & Torres–Peimbert (1974, 1976) outlined a programme whereby measurements in Galactic and extragalactic HII regions having different Z abundances (represented mainly by oxygen, although sometimes nitrogen is used, too) could be used to plot a regression represented by

$$Y = Y_P + Z\frac{\Delta Y}{\Delta Z} = Y_P + ({\rm O/H})\frac{\Delta Y}{\Delta({\rm O/H})}. \qquad (2.14)$$

Extrapolation to $Z = ({\rm O/H}) = 0$, would give the primordial helium abundance Y_P, while the slope of the regression, $\Delta Y/\Delta Z$ (not necessarily constant) would place a

[5]It is worth mentioning that helium was first discovered in 1868 by Pierre Janssen and subsequently confirmed by Norman Lockyer and Edward Frankland by observing the chromosphere of the Sun during a solar eclipse.

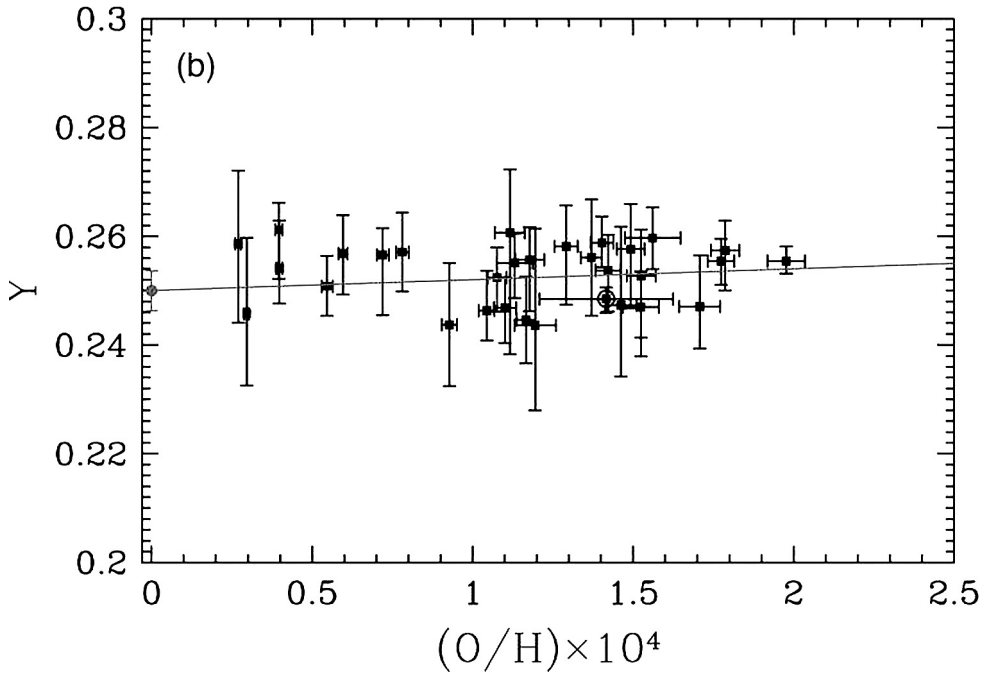

Figure 2.3: *Helium mass fraction Y vs. oxygen abundances* $\mathrm{O/H}$ *for 30 metal–poor HII regions, when the effect of stellar absorption is taken into account. The resulting slope is* $\Delta Y/\Delta(\mathrm{O/H}) = 20 \pm 25$ *which corresponds to* $\Delta Y/\Delta Z = 1.1 \pm 1.4$ *(Fukugita & Kawasaki 2006).*

significant constraint on stellar nucleosynthesis, by giving the rate at which helium is freshly synthesised and ejected into the InterStellar Medium (ISM) compared to the corresponding rate for metals. The application of this idea to objects in our own Galaxy suffers from the fact that the abundances represented by Z are rather high, so that a large extrapolation is needed to obtain an estimate of Y_P. In addition, planetary nebulae need a small correction for helium dredged up to the surface during prior stellar evolution, while Galactic HII regions mostly have ionizing stars that are not hot enough to guarantee the absence of otherwise undetectable neutral helium. Consequently, the best objects in which to apply this idea are extragalactic HII regions in dwarf irregular galaxies and in blue compact galaxies, where the abundances of oxygen and other heavy elements are low and the ionizing stars often very hot. It is worth mentioning that the occurrence of a complete ionization is however a rather ideal case also for extragalactic HII regions (e.g. Viegas, Gruenwald & Steigman 2000). The present inventory of such regions studied for their helium content exceeds 80 (Izotov & Thuan 2004; Izotov, Thuan & Stasińska 2007), although often a posteriori selected subsample is used in order to determine Y_P.

Over the last fifteen years there has been a considerable trend in the estimated value

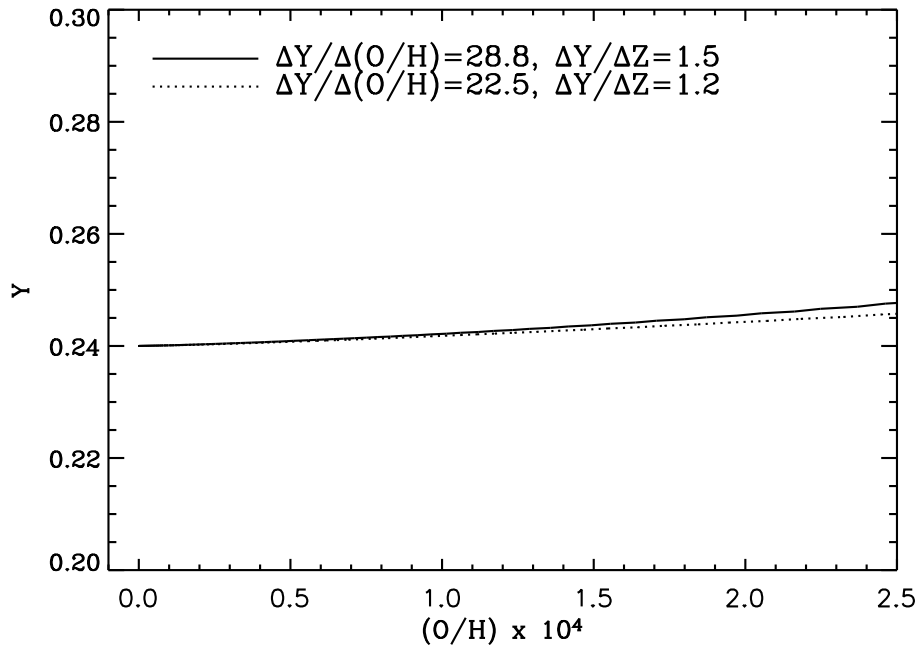

Figure 2.4: *Helium mass fraction Y vs. oxygen abundances* $\mathrm{O/H}$ *from the chemical evolution models presented in Chapter 4. Continuous line refers to model A (built to match the mean observational constraints in the Solar Neighbourhood) and dotted line to model B (appositely selected to reach high metallicities at the present time of 13 Gyr). The gradients* $\Delta Y/\Delta(\mathrm{O/H})$ *and* $\Delta Y/\Delta Z$ *are computed for the same range of the data in Figure 2.3. Notice that in the chemical evolution models* $Y_P = 0.24$ *has been assumed.*

of Y_P, from a "low" primordial helium abundance ($Y_P = 0.228 \pm 0.005$ Pagel et al. 1992; $Y_P = 0.234 \pm 0.002$ Olive, Skillman & Steigman 1997; $Y_P = 0.2391 \pm 0.0020$ Luridiana et al. 2003) to a "high" primordial helium abundance in better agreement with Y_P computed assuming standard BBN and η_{10} from CMB ($Y_P = 0.2421 \pm 0.0021$ Izotov & Thuan 2004; $Y_P = 0.249 \pm 0.009$ Olive & Skillman 2004; $Y_P = 0.250 \pm 0.004$ Fukugita & Kawasaki 2006; $Y_P = 0.2477 \pm 0.0029$ Peimbert, Luridiana & Peimbert 2007; $Y_P = 0.2516 \pm 0.0011$ Izotov, Thuan & Stasińska 2007). The lesson from the above determinations is that although recent attempts to determine the primordial abundance of $^4\mathrm{He}$ have achieved high precision, their accuracy remains in question. The latter is limited by the understanding of and ability to account for systematic corrections and their errors, not by statistical uncertainties. The convergence of the measured primordial helium abundance to a closer agreement with that predicted assuming standard BBN and the measured baryon–to–photon ratio hopefully reflects a better understanding of the complex physics of HII region and not a forcing of the data.

The most recent analyses (Olive & Skillman 2004; Fukugita & Kawasaki 2006; Peimbert, Luridiana & Peimbert 2007) fail to find evidence for the anticipated correlation between the helium and the oxygen abundance (Figure 2.3), calling into question the model–dependent extrapolations to zero metallicity often employed in the quest for primordial helium. The theoretical correlation between helium and oxygen abundance is addressed in Figure 2.4 by means of the chemical evolution model presented in Chapter 4. Interestingly, the very flat evolution of Y compared to oxygen observed by Fukugita & Kawasaki (2006) is confirmed by our chemical evolution model. Although the observed correlation is obtained studying HII regions, and our model is best suited to describe the evolution of the Galactic disc, the predictions are rather insensitive to the detail of the model calibration, as we discuss in more details in Chapter 4.

According to Steigman (2007) all the analyses presented to date have different sort of systematic errors. In particular, because hydrogen and helium recombination lines are used, the observations are blind to any neutral helium or hydrogen, which are anyway present. Estimates of the ionization correction factor are unfortunately model dependent and possibly also very large (Viegas, Gruenwald & Steigman 2000; Gruenwald, Steigman & Viegas 2002). The value proposed by Steigman (2007) for the primordial helium abundance is

$$Y_P = 0.240 \pm 0.006 \tag{2.15}$$

where the adopted error is an attempt to account for the systematic as well as the statistical uncertainties. We adopt this value for the composition of the protogalactic gas cloud used in the chemical evolution model presented in Chapter 4.

CHAPTER 3

Fine Structure in the Lower Main-Sequence

"Stars shining bright above you"

Dream a Little Dream of Me – Gus Kahn

3.1 Quasi–homology relations

We have already stated that the main goal of this thesis is to carefully derive physical parameters for low mass stars in order to gauge insight into the chemical evolution of helium. Performing such a task using nearby stars has always proved challenging and all studies to date have exploited the fact that the broadening of the lower main-sequence with metallicity effectively depends on the helium content (e.g. Faulkner 1967; Strömgren, Olsen & Gustafsson 1982; Fernandes, Lebreton & Baglin 1996; Pagel & Portinari 1998; Jimenez et al. 2003). To this purpose, precisely locating low mass stars on the HR diagram is crucial, as we discuss in what follows.

For stars still on their zero-age main-sequence, it is well known that an increase of helium (Y) keeping the metallicity (Z) constant induces an increase of luminosity ($M_{\rm Bol}$) and effective temperature ($T_{\rm eff}$) at a given mass. On the other hand an increase of Z at fixed Y leads to the opposite effect, i.e. luminosity and effective temperature decrease (e.g. Fernandes, Lebreton & Baglin 1996). This behaviour is clearly shown in Figure 3.1 plotting some of the tracks and isochrones used in Paper II. Figure 3.1 also highlights how the broadening of the lower main-sequence is independent of the age and how the shift at a fixed mass with increasing age is rather small and into a direction parallel to the main-sequence.

Such a behaviour is due to opacity and mean molecular weight effects and can be easily explained in the framework of quasi–homology theory which we briefly review here. A thorough discussion can be found e.g. in Cox & Giuli (1968). Using the quasi–homology relations, luminosity and effective temperature of a main-sequence star can be expressed as

$$L = \epsilon_0^{-0.077} \kappa_0^{-1.077} \mu^{7.769} M^{5.462} \tag{3.1}$$

$$T_{\rm eff} = \epsilon_0^{-0.096} \kappa_0^{-0.346} \mu^{2.211} M^{1.327} \tag{3.2}$$

where $\mu = (2X + 0.75Y + 0.5Z)^{-1}$ is the mean molecular weight (complete ionized gas), ϵ_0 the nuclear energy generation rate, κ_0 the opacity and M the stellar mass. By

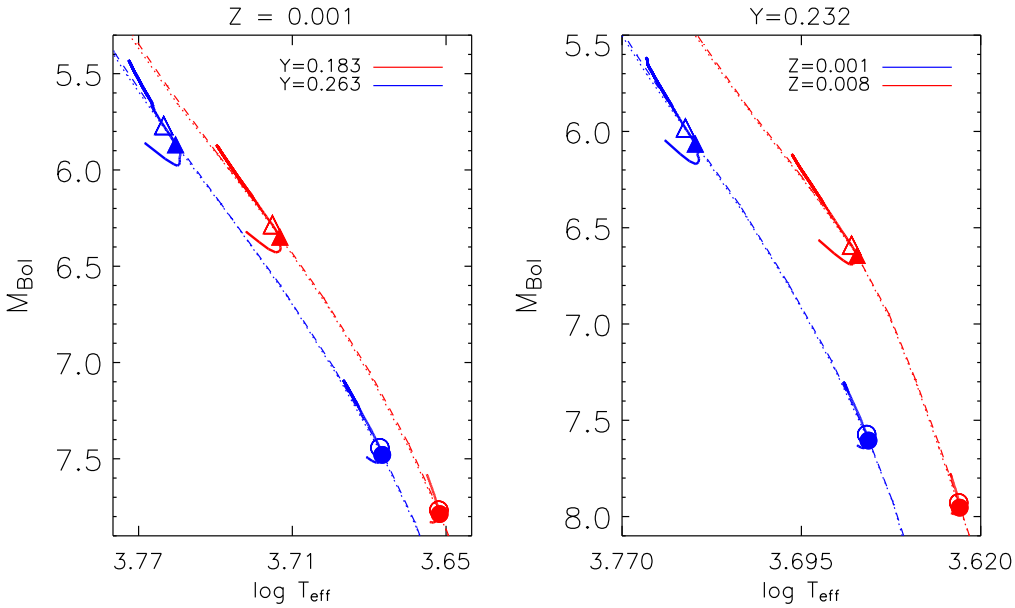

Figure 3.1: *Left panel: change in $M_{\rm Bol}$ and $T_{\rm eff}$ with increasing Y for a fixed Z. Right panel: change in $M_{\rm Bol}$ and $T_{\rm eff}$ with increasing Z for a fixed Y. Thick lines are stellar tracks at two given masses ($0.7\,M_{\odot}$ and $0.5\,M_{\odot}$) whereas dotted and dashed lines are the isochrones built interpolating the stellar tracks at the ages of 1 Gyr and 5 Gyr, respectively. Filled (open) triangles refer to $0.7\,M_{\odot}$ at an age of 1 Gyr (5 Gyr). Filled (open) circles refer to $0.5\,M_{\odot}$ at an age of 1 Gyr (5 Gyr).*

combining equations (3.1) and (3.2) and making some simplifying assumptions on the form of $\epsilon_0 \propto X^2$ (i.e. main source of energy through pp-chain, where X is the hydrogen mass fraction) and $\kappa_0 \propto (1+X)(100Z+1)$ (i.e. opacity dominated by bound-free and free-free transitions) it is possible to find an analytical formula between the luminosity and the effective temperature, which depends only on the stellar chemical composition X, Y, Z. Further assuming that

$$Y = Y_0 + Z\frac{\Delta Y}{\Delta Z} \tag{3.3}$$

and since $X + Y + Z = X_0 + Y_0 = 1$ it follows that

$$X = 1 - Y - Z = X_0 - Z\left(\frac{\Delta Y}{\Delta Z} + 1\right) \tag{3.4}$$

and thus and entire family of luminosity–$T_{\rm eff}$ relations can be built by simply scaling the chemical composition with Z as a function of $\Delta Y/\Delta Z$. For a given chemical composition, the resulting luminosity–$T_{\rm eff}$ relation effectively acts like an isochrone

$$L \propto (X + 0.4)^{2.67}(100Z + 1)^{0.455} f(T_{\rm eff}). \tag{3.5}$$

By choosing a reference luminosity–$T_{\rm eff}$ relation is then possible to compute the difference in luminosity (or effective temperature) for all the other relations as function of Z and $\Delta Y/\Delta Z$ only (e.g. Pagel & Portinari 1998).

3.2 Two recent works on $\Delta Y/\Delta Z$ from low mass stars

The formalism previously introduced provides a physical ground to understand the broadening of the lower main-sequence in terms of stellar helium and metal content. However, for a better comparison with the observational data, theoretical isochrones derived from the latest stellar models are usually used.

Among various works done in the past, two in particular have tackled the question in great details, Pagel & Portinari (1998) and Jimenez et al. (2003). By using the formalism previously introduced, Pagel & Portinari (1998) numerically derived fitting formulae linking the difference in effective temperature ($\Delta \log T_{\rm eff}$) from a reference isochrone as function of Z and $\Delta Y/\Delta Z$ using a set of Padova isochrones. The reference isochrone was chosen to be the solar one. Their sample included about thirty K dwarfs with *Hipparcos* parallaxes which were studied in the $M_V - \log T_{\rm eff}$ plane, using effective temperatures derived via the InfraRed Flux Method (IRFM) from Alonso, Arribas & Martínez-Roger (1996). They found $\Delta Y/\Delta Z = 3 \pm 2$.

Jimenez et al. (2003) used a rather similar approach. Also in this case the sample was composed by approximately thirty K dwarfs for which accurate parallaxes obtained with the *Hipparcos* satellite were available. The analysis was performed in the $M_V - (B-V)$ plane, exploiting the difference in luminosity (ΔM_V) with respect to a reference isochrone, which they chose to be the primordial one. They assumed a value for the primordial helium Y_0 and computed different models for various Z and $\Delta Y/\Delta Z$. For both models and sample stars ΔM_V was computed with respect to the reference isochrone. Since all the isochrones with difference helium abundances at a given Z were computed starting from the same Y_0, the effect of different helium enhancements became relevant only at the highest metallicities which had most of the leverage in determining the final result $\Delta Y/\Delta Z = 2.1 \pm 0.4$.

3.3 $\Delta Y/\Delta Z$ in nuce

The motivating idea behind this thesis was to determine the broadening of the lower main-sequence with precision greater than ever before, so as to provide the most stringent determination yet of $\Delta Y/\Delta Z$ from lower main-sequence stars. Collecting a larger dataset of highly accurate and homogeneous observational data on K dwarfs, together with the choice of working directly in the $M_{\rm Bol} - T_{\rm eff}$ plane (where the effect of the helium is more pronounced, e.g. Castellani, degl'Innocenti & Marconi 1999) has been the driving idea of the project and the motivation beyond Paper I. In this paper, we have

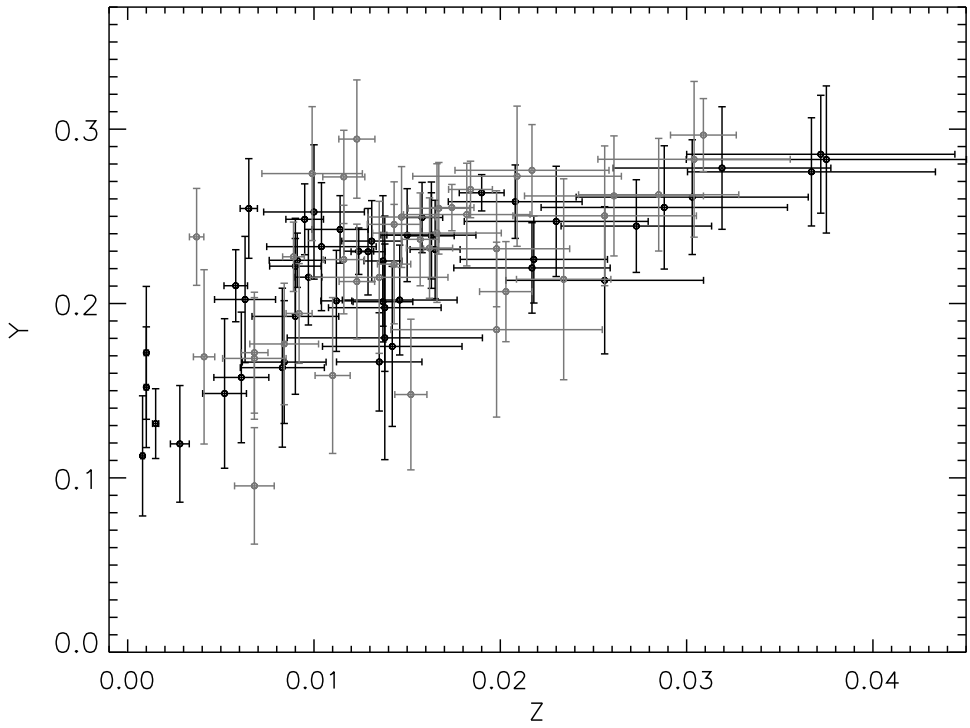

Figure 3.2: *Helium (Y) to metal (Z) enrichment factor obtained in Paper II. For metallicities slightly below solar ($Z_{\odot} = 0.017$) extremely low helium abundances are found.*

developed our own version of the IRFM to recover the fundamental stellar parameters from multi–band photometry.

A new set of low mass stellar tracks, computed especially for us at Padova, for various metallicities and helium abundances has been used to derive $\Delta Y/\Delta Z$ from the new sample (Paper II). Theoretical stellar models have a number of free parameters usually calibrated on the Sun. One of this parameters is the helium mass fraction, which automatically fixes the hydrogen mass fraction, since that of the metals comes from observations (although its correct value is currently a matter of debate, e.g. Basu & Antia 2008 for a review). Therefore, when dealing with theoretical stellar models, the abundances introduced in equations (3.3) and (3.4) must be intended as calibration parameters, the exact value of which varies depending on the input physics implemented in the adopted stellar evolutionary code.

For this reason, X_0 and Y_0 introduced here do not necessarily correspond to the primordial hydrogen and helium mass fraction presented in the previous Chapter. The choice of the calibration parameters is simply a zero-point effect, which is irrelevant when dealing with a differential quantity such as $\Delta Y/\Delta Z$ and thus it justifies both ap-

proaches used in Pagel & Portinari (1998) or Jimenez et al. (2003), who adopted different reference isochrones in their studies. In our work (Paper II) we chose to use the solar isochrone as the reference one, since it is the calibration zero–point of stellar models; however, comparison with other isochrones sets, including that of Jimenez et al. (2003) with a fixed primordial isochrone, did not affect our results.

Working in the theoretical HR diagram allowed us to highlight shortcomings in the low-metallicity theoretical stellar models, which unfortunately precluded us from deriving $\Delta Y/\Delta Z$ over the entire Z range represented by stars in the Solar Neighbourhood. Starting from metallicities slightly below solar, we have found that anomalously low helium abundances (well below the primordial value) are needed to reproduce the data (Figure 3.2), namely theoretical isochrones are too hot with respect to observations. Besides accounting for non-local thermodynamic equilibrium (LTE) in deriving metallicities, including diffusion in stellar models partly helps to solve the problem. Such a conclusion can be interpreted as an independent hint for diffusion acting also in nearby metal–poor field stars, corroborating the evidence already seen in globular clusters (Korn et al. 2006). Although helping, both non-LTE and diffusion seem not enough to entirely solve the low helium problem and a mixing–length decreasing with decreasing metallicity has also been proposed in Paper II. Therefore, at present it is not yet possible to derive $\Delta Y/\Delta Z$ from stellar models at low Z. The result obtained in Paper II was thus limited to stars with metallicities around and above the solar one. However, the technique presented in Paper I to recover effective temperatures and bolometric luminosities of low mass stars has been further improved and developed so to be successfully applied also to M dwarfs (Paper III). The relevance of the results obtained throughout this thesis in the more general context of studies dealing with Galactic Chemical Evolution are outlined in the next chapters.

CHAPTER 4
The chemical evolution of helium

"For the things we have to learn before we can do them, we learn by doing them"

Aristotle

4.1 The overall picture

The small ripples observed in the CMB (e.g. Spergel et al. 2003, 2007) are the seeds of the galaxies which form the LSS of the Universe. In the currently accepted framework, the dynamic of the LSS is dominated by dark matter and dark energy. In this very schematic picture, the baryons left from the Big Bang in the form of H, D, ^{3}He, ^{4}He and ^{7}Li (see Chapter 2) collapse in the potential well of the dark matter haloes (e.g. White & Rees 1978) to eventually form the stars and the galaxies we observe today. The actual process of galaxy formation is considerably more complicated and involves highly non-linear processes, so that only detailed numerical simulations can tackle them —at least to some extend. The ultimate goal of a successful theory of galaxy formation is to be able to understand and describe the formation and the evolution of the various components (stellar and non) which characterize different types of galaxies, observed at various redshifts. In this quest, our Galaxy, the Milky Way, offers a formidable nearby template where to test and calibrate some of the various ingredients needed for a self-consistent theory of galaxy formation. The purpose of Galactic Chemical Evolution (GCE) models is exactly to focus on some (or as many as possible) of those processes responsible for the chemical enrichment of the Milky Way as deduced from the abundances observed in stars and gas. GCE models thus specifically deal with the chemistry of the Galaxy, highly simplifying the complex dynamic involved in its formation.

Figure 4.1 shows a sketch of the Milky Way, seen edge-on. Several components consisting of stars and gas with various properties as regards kinematics and chemical composition are present. The stellar populations of these main components, halo, bulge and disk, have quite different chemical compositions, kinematic and dynamical properties reflecting different evolutionary histories. Traditionally, two scenarios have competed to explain the formation of the Milky Way. The first one, proposed by Eggen, Lynden-Bell & Sandage (1962), describes the rapid monolithic collapse of a protogalactic gas cloud to form the halo. The Galactic disk wold have subsequently formed as the residual gas dissipationally collapsed, spun up due to conservation of angular momentum. This would naturally give rise to two populations of stars: an older, more metal–poor group found in the halo, and a younger, more metal–rich group orbiting closer to the Galactic

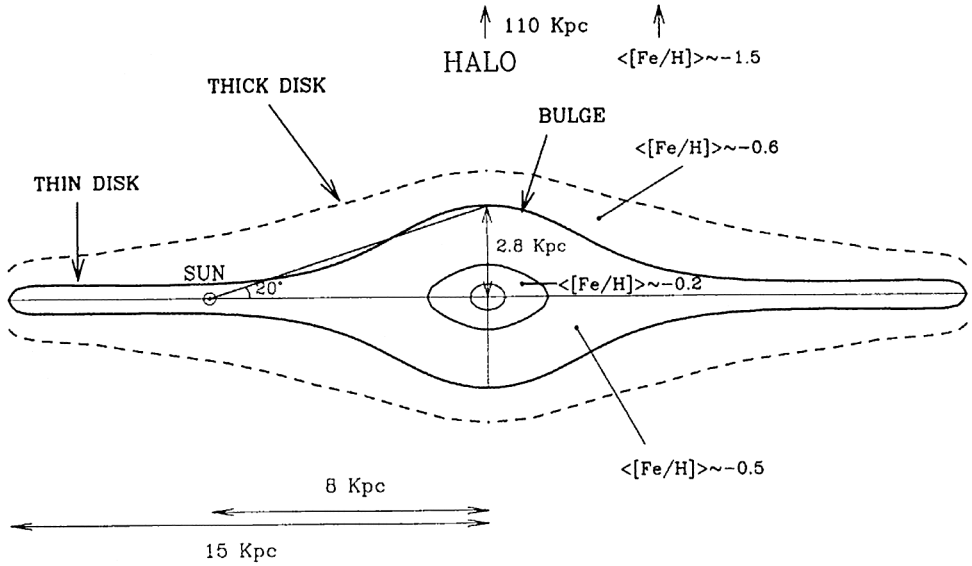

Figure 4.1: *A sketch of the structure of the Milky Way: the stellar halo, bulge, thick and thin disk are indicated together with the mean metallicity of the stars in each Galactic component. The galactocentric distance of the Sun together with the dimension of the optical disk are shown at the bottom (from Matteucci 2001).*

mid–plane. Searle & Zinn (1978) offered an alternative to the monolithic collapse picture, proposing that the Galaxy was constructed from smaller cloud fragments, in which stars may have already started forming.

The Galaxy's true formation history is likely to lie somewhere between the two extremes of primordial collapse and hierarchical formation, in the more general framework of ΛCDM structure formation (e.g. Freeman & Bland-Hawthorn 2002; Chiosi 2007). The recent evidence that the halo of the Milky Way is composed by two populations, the inner and the outer halo, with distinct kinematic properties and metallicity distribution functions, further confirms such a conclusion (Carollo et al. 2007).

Independent of the exact details of this picture, galaxy formation is accompanied by star formation leading to synthesis of heavier elements and modification of primordial abundances: D is destroyed by stellar activity, ^{4}He is mildly topped up and ^{3}He and ^{7}Li are both created and destroyed by stars (e.g. Chiappini, Renda & Matteucci 2002; Romano et al. 2003; Carigi & Peimbert 2008).

When stars are formed, there are broadly few things that can happen to the ISM as a result of their evolution. Galactic Chemical Evolution models deal specifically with the stellar evolutionary processes so as to explain the chemical composition observed in

stars and gas in the Galaxy. Stars of different mass ranges give different contribution to the chemical evolution of the Galaxy, as summarized below. There are still uncertainties in the exact boundaries of the stellar mass ranges discussed below, also depending on the stellar metallicity and whether or not stellar models with convective overshooting are employed. In the present introduction, we aim to give a qualitative overview.

Very low mass stars, with $M < 0.8\,M_{\odot}$ have such long lifetimes that they essentially do nothing: they simply serve to lock up part of the gas and remove it from circulation, but they remain visible today as archaeological tracers of the composition of the ISM at the time and place where they formed. These stars can be used to trace the chemical evolution of the Milky Way. Their characterization is the subject of Paper I and III and their study by means of theoretical stellar models is presented in Paper II. In particular, one of the basic assumptions is that the chemical composition in the atmospheric layers of such stars is representative of the gas out of which the stars once formed, i.e. no processes substantially altered their chemical composition at the surface with time. Such an assumption is of paramount importance for chemical evolution studies and it has been partly discussed also in Paper II.

Low and Intermediate mass stars, approximately from 0.8 to 5 $M_{\odot}$ —in models with convective overshooting— undergo various dredge–up and mass loss episodes as they evolve after the main-sequence and pass through the Red Giant Branch (RGB), the Horizontal Branch (HB), the Asymptotic Giant Branch (AGB) and the Planetary Nebula (PN) phases before they end up as CO–white dwarfs. Low mass stars, with mass below about 2 $M_{\odot}$ (e.g. Maeder & Meynet 1989; Chiosi, Bertelli & Bressan 1992) ignite helium in an electron degenerate core (He flash), whereas above this mass intermediate mass stars avoid the core helium flash and burn He quiescently. Close binaries in this mass range can undergo more dramatic events as a result of mass transfer. In particular, they can explode as supernovae Ia which contribute substantially to the nucleosynthesis of iron and explain the observed evolution of the abundance ratio of α–elements with respect to [Fe/H] (e.g. Sneden et al. 1979; Matteucci & Greggio 1986; McWilliam 1997).

Quasi massive stars, in the range $\sim 5 - 8\,M_{\odot}$ undergo core C–burning in non degenerate conditions, but develop highly degenerate O-Ne-Mg–cores. They become dynamically unstable and are thought to explode as electron capture supernovae, although their final state is still a matter of debate. Super–Asymptotic Giant Branch evolution might alternatively develop in the non–violent formation of a massive white dwarf, or in a weak explosion at most (Ritossa, Garcia-Berro & Iben 1996; Eldridge & Tout 2004).

Massive stars, in the range $\sim 8 - 120\,M_{\odot}$, have simultaneous occurrence of two phenomena: the dominant mass loss by stellar wind during the whole evolutionary history (significant especially above $30\,M_{\odot}$) and the completion of the nuclear sequence down to the formation of an iron core in presence of strong neutrino cooling. These stars end up as Type II supernovae or Type Ib,c supernovae if the progenitor suffered from effective mass loss and lost its H–rich envelope before the explosion. Either a neutron star or a black hole is left over.

Very massive stars i.e. objects more massive than $\sim 120\,M_{\odot}$ are strongly pulsationally unstable and suffer from violent mass loss. The final outcome is regulated by the mass of the CO–core: these stars can either collapse to a black hole, suffer from complete thermonuclear explosion or recover the behaviour of the massive stars above.

The net result of the stellar evolution schematically outlined above is clear: it is to change the initial Galactic chemical composition. The purpose of GCE models is to interpret all these processes within the bigger framework of the stellar populations which compose the Galaxy, so as to account for the abundances observed in stars and gas. Obviously, the larger the number of observables, the more the framework provided by GCE can be useful in constraining the history of the Milky Way. In particular, for obvious reasons, the Solar Neighbourhood is the best observed system.

4.2 $\Delta Y/\Delta Z$ from different stellar populations

In order to trace the history of chemical evolution it is quite important to analyze in detail the nucleosynthesis of various elements taking place in stars with different masses and metallicities. Following the classical definition by Tinsley (1980), the stellar yield, $p_i(M, Z)$ of a given element i, is the mass fraction of a star with initial mass M and metallicity Z that is converted into the element i and returned to the ISM during its entire lifetime. Stellar yields are thus important for studies of the chemical evolution of the galaxies.

In this Section we address the topic more specifically, considering the global yields of a stellar population born with a typical Solar Neighbourhood Initial Mass Function (IMF). The inclusion of the stellar yields in our chemical evolution model will be the subject of the next Section. The yields adopted in the present study are those of Portinari, Chiosi & Bressan (1998) for massive stars ($6 < M < 120 M_{\odot}$) and Marigo (2001) for intermediate and low mass stars ($0.8 < M < 5 M_{\odot}$). Both Portinari et al. (1998) and Marigo (2001) stellar yields are based on the Padova evolutionary tracks. The range in metallicity covers from $Z = 0.0004$ to $Z = 0.05$. In Section 4.2.1 we compare the adopted yields with other sets which have recently appeared in literature and we justify our choice.

In Figure 4.2 the adopted stellar yields have been properly weighted by a chosen IMF; we mainly adopt the IMF by Kroupa (1998), and we discuss later the differences when assuming e.g. the Salpeter (1955) IMF. At low Z, helium is produced mostly by stars in the mass range $0.8 < M < 10\,M_{\odot}$. The peak of helium production around $2 - 3\,M_{\odot}$ is mostly due to dredge-up episodes during the Thermally Pulsating Asymptotic Giant Branch (TP-AGB), whereas the contribution at $4 - 5\,M_{\odot}$ is caused by the additional occurrence of Hot Bottom Burning (HBB) in addition to dredge-up episodes during the TP-AGB. In this mass range, the production of helium is more pronounced at the lowest metallicities when the number of stellar pulses is larger and the TP-AGB duration longer (e.g. Marigo 2001). More massive stars have minor importance in the

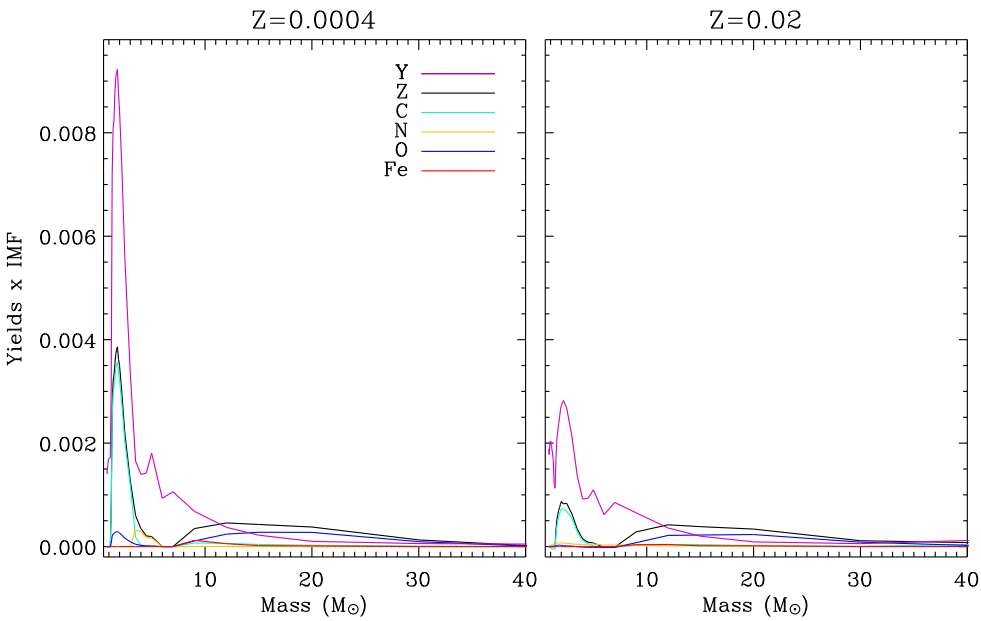

Figure 4.2: *Stellar yields in helium and heavy elements, weighted by the IMF (Kroupa) for models with two different initial metallicities ($Z = 0.0004$ and $Z = 0.02$)*

production of helium, especially at low Z. With increasing metallicity, however, stellar wind and mass loss in massive stars become important, so that the contribution of metal–rich massive stars to the production of helium is more relevant. The production of C also peaks around $2 - 3\,M_{\odot}$, corresponding to the largest number of dredge-up episodes during the TP-AGB phase, provided that HBB has not operated. The subsequent decline towards higher masses is initially due to fewer dredge-up events, and then to the prevailing effects of HBB. The contribution of massive stars to the enrichment of C increases with metallicity due to more efficient mass loss. At low metallicities N is mostly produced during the HBB in intermediate mass stars, while at higher metallicities secondary production of N via the CNO cycle occurs over the whole mass range. O is mainly produced by massive stars at all metallicities, with a minor contribution from stars with $M < 3.5\,M_{\odot}$ thanks to the dredge-up events during the TP-AGB phase. In this Figure Fe comes from Type II supernovae; the other main contribution, from Type Ia supernovae, will be included only in the chemical evolution model.

While the global metallicity Z is mostly produced by massive stars, with low and intermediate mass stars contributing some 15–40% (at Z=0.02 and Z=0.0004 respectively), the latter give a relevant contribution to helium enrichment: from about 60% at low Z, to 40% at metallicities around solar. Therefore helium is partly produced on longer timescales than the metals Z, a behaviour qualitatively reminding the trend of

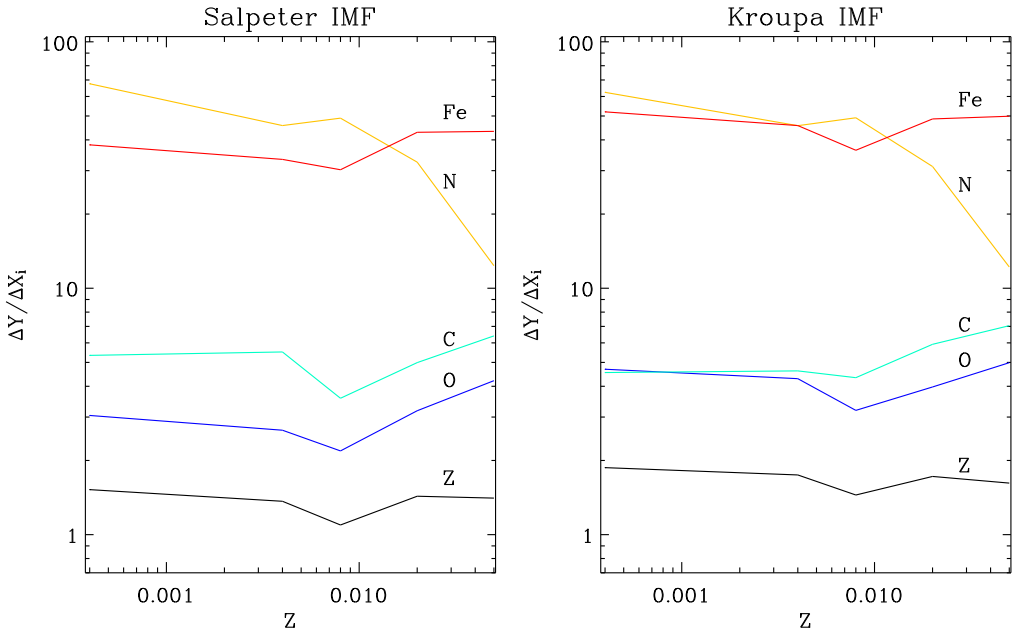

Figure 4.3: *$\Delta Y/\Delta X_i$ where X_i is the total metal mass fraction (Z) or the mass fraction of specific elements (*C, N, O, Fe*) plotted as function of the metallicity Z covered by the adopted stellar yields. $\Delta Y/\Delta X_i$ is computed integrating over the entire stellar population weighted by a given IMF (Salpeter or Kroupa). Notice that* Fe *is here produced by Type II supernovae only. The inclusion from supernovae of Type Ia is done in the GCE model presented in the next Section.*

[α/Fe] ratios.

Figure 4.3 shows the helium–to–metal enrichment ratio when Z or the mass fraction of other elements (C, N, O, Fe) is considered. The curves result from the adopted stellar yields when they are integrated over the entire stellar population (i.e. from 0.1 to 120 $M_{\odot}$ although only masses above $0.8M_{\odot}$ contribute) and weighted by two different IMFs, the Salpeter (1955) and Kroupa (1998). Choosing between different IMFs obviously changes the global $\Delta Y/\Delta X_i$ as different proportions of massive or low and intermediate mass stars are involved (e.g. Chiosi & Matteucci 1982).

The global $\Delta Y/\Delta Z$ expected to be produces by a stellar population with the Kroupa IMF is between 1.8 and 1.4; this is somewhat lower, but comparable to our observational result of $\Delta Y/\Delta Z \simeq 2$. With the Salpeter IMF, which has a shallower slope and hence a smaller percentage of low and intermediate mass stars, the expected $\Delta Y/\Delta Z$ is lower, between 1.5 and 1. Therefore adopting the Kroupa (1998) IMF for our GCE models of the Solar Neighbourhood has a better chance to recover the observed value; notice however that the difference with respect to the Salpeter IMF is at the same level as the current observational accuracy.

4.2.1 Comparison with other chemical yields

Although other sets of yields have been recently published (e.g. Ventura, D'Antona & Mazzitelli 2002; Maeder & Meynet 2002; Hirschi, Maeder & Meynet 2005; Karakas & Lattanzio 2007), these are restricted to mass and metallicity ranges much smaller than those used in our GCE model, so that to use them one should patch yields computed by various authors. The occurrence of important nucleosynthesis processes in certain mass and metallicity ranges depends upon the physics implemented in different stellar codes (e.g. convection model used, method for determining the convective borders, inclusion of overshooting). It is therefore obvious that taking yields from different authors can introduce a source of inaccuracy which is avoided when adopting the complete and homogeneous set of Padova yields. Nonetheless, we compare here our adopted set with other recently published, to check if that would make any major difference in our final results.

Karakas & Lattanzio (2007) have recently computed stellar yields for 74 chemical species at various metallicities (from $Z = 0.0001$ to $Z = 0.02$) in the mass range $1 - 6\,M_{\odot}$. Stars in this mass range undergo various evolutionary stages, in particular the TP-AGB phase, whose modeling is still a difficult task, due to both the high complexity of the physics involved and the remarkable requirement of computing time (e.g. Marigo 2001; Marigo & Girardi 2007; Karakas & Lattanzio 2007). A viable approach is offered by synthetic models, which summarize the results of complete stellar calculations through simple and practical analytical relations depending upon few parameters. The parameters used in the synthetic models of Marigo (2001) are calibrated to reproduce fundamental observables (e.g. the carbon stars luminosity function, the initial-final mass relation of low and intermediate mass stars) whereas those computed by Karakas & Lattanzio (2007) are not. The main difference is a deeper third dredge-up in the Marigo (2001) models, so that Karakas & Lattanzio (2007) produce a lower amount of metal, C, N and particularly O, as well as less helium (see also the detailed comparison presented in Karakas & Lattanzio 2007). When the yields are integrated over the entire stellar population from 1 to $6M_{\odot}$ and weighted by the Kroupa (1998) IMF, the $\Delta Y/\Delta Z$ from Karakas & Lattanzio (2007) varies from about 4.5 to 8.7, whereas the yields from Marigo (2001) predict a shallower slope ranging from 2.8 to 4.6, depending on the metallicity.

For massive stars, a recent set of yields is that available from the Geneva group (Maeder & Meynet 2002; Hirschi et al. 2005) which also takes into account the effect of stellar rotation. These yields are presently given for three metallicities ($Z = 10^{-5}, 0.004$ and 0.02) in the mass range $\sim 10 - 60\,M_{\odot}$. A throughout comparison between rotating and non-rotating models is given in the original papers. Briefly, CNO yields from rotating models are usually slightly higher than those from non-rotating models whereas the helium production is rather similar, thus implying only a moderate decrease in $\Delta Y/\Delta Z$ for the rotating case. With respect to the yields of Portinari et al. (1998), the rotating yields predict a similar $\Delta Y/\Delta Z$ at $Z = 0.004$, whereas it decreases to almost half at solar metallicity. What is important in rotating models is the effect of stellar winds, espe-

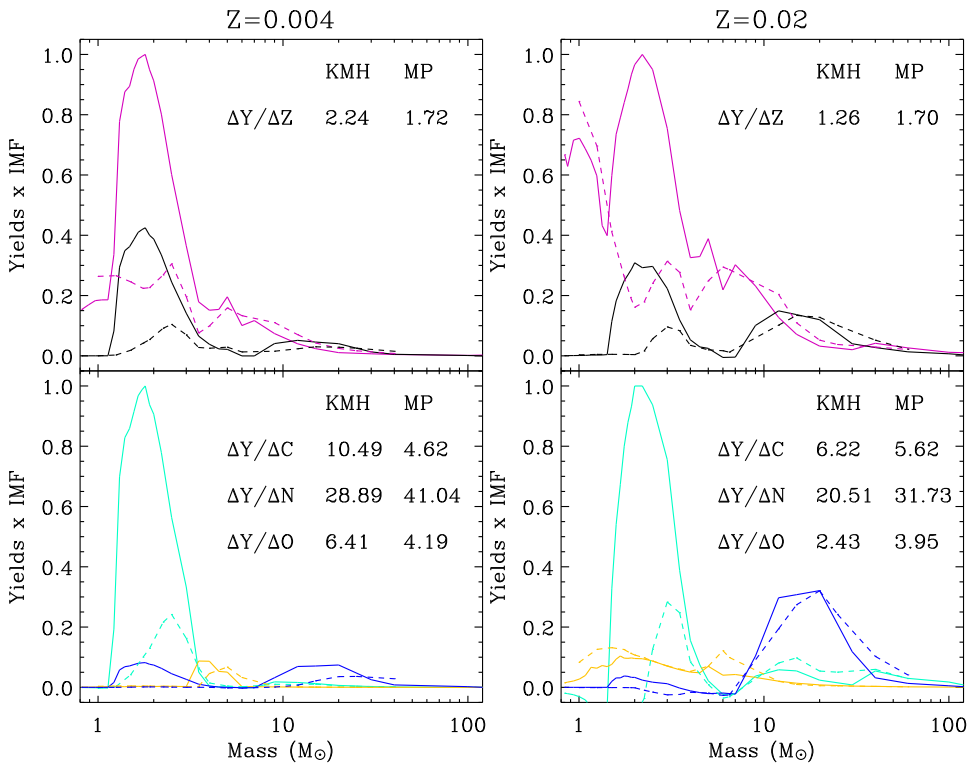

Figure 4.4: *Comparison between the yields from Marigo (2001) and Portinari et al. (1998) represented by continuous lines (MP) and a patchwork including the yields from Karakas & Lattanzio (2007), Maeder & Meynet (2002) and Hirschi et al. (2005) instead (KMH, dashed lines). The comparison is shown for two different metallicities. The upper panels show the helium (purple) and Z (black) yields, whereas the lower panels display the* C *(cyan),* N *(yellow) and* O *(blue) yields. Also reported are the helium to various elements enrichment ratios obtained integrating over the entire stellar population at the metallicity given in each plot. A Kroupa (1998) IMF is assumed. The peak in each plot is normalized to one and a logarithmic scale is used for the mass in order to facilitate the comparison.*

cially at extremely low metallicities ($Z = 10^{-8} - 10^{-5}$) which should be representative of the —yet unobserved— first stars responsible for the early chemical evolution of the Galaxy. Whereas the yields (i.e. the total contribution from stellar winds plus supernova explosions) from rotating and non-rotating models are similar, the efficient mixing in rotating models enriches considerably the stellar surface which in turn favours a large mass loss by stellar wind (rich in helium), whereas the supernova contribution is greatly diminished (Meynet, Ekström & Maeder 2006). *Ad hoc* scenarios in which the winds of high mass stars drive the chemical evolution without the contribution in heavy elements from supernovae are worth investigating to explain e.g. the anomalous abundance pat-

terns observed in ω Centauri (Maeder & Meynet 2006), but this is clearly outside the purpose of the present study.

Figure 4.4 shows the stellar yields in helium and heavy elements when a patchwork including yields from Karakas & Lattanzio (2007) below $6\,M_{\odot}$ and the high mass rotating yields from Maeder & Meynet (2002) and Hirschi et al. (2005) is used instead of the yields presented in Section 4.2 and adopted in our GCE model. Despite the differences in the adopted sets, when the yields are integrated over the entire mass range, the ratios reported in Figure 4.4 compare quite nicely. Especially for $\Delta Y/\Delta Z$ the difference is about 30%, substantially at the same level as the current observational accuracy; it is lower at low Z, higher at high Z for the Padova yields compared to more recent ones. Such a conclusion ensures that our results do not depend too critically on the specific set of yields employed. In addition, the fact that the TP-AGB phase in our yields is empirically calibrated is a fundamental additional constraint and since all our adopted yields are computed using the same Padova stellar evolutionary code, this ensures a greater homogeneity in our final results.

4.3 A model for the chemical evolution of the Galaxy

We have previously outlined the main stellar populations which compose the Galaxy and their contribution in driving its chemical evolution. However, to put together a model for the chemical evolution of the Galaxy, one still needs to combine the following ingredients.

- The Star Formation Rate (SFR), i.e. a measure of the typical timescale and mass of gas that goes into stars, usually quantified in terms of $M_{\odot}\mathrm{pc}^{-2}\mathrm{Gyr}^{-1}$. Besides the assumption of a constant SFR, the simplest possible parametrization of the SFR is to assume that it is just proportional to the surface density of gas.

- The Initial Mass Function (IMF) i.e. the relative number of stars with different initial mass $mM_{\odot}$ in a given interval dm.

- The stellar ejecta of different elements, i.e. a budget of the products of stellar evolution.

Here we briefly summarize the main features of our chemical evolution model, which we apply to the Solar Neighbourhood. Full details are available in Portinari et al. (1998).

An open model with continuous infall of primordial gas that builds the disk gradually is adopted. Such a process is supported by dynamical studies (e.g. Larson 1974, 1976; Carraro, Lia & Chiosi 1998; Sommer–Larsen, Götz & Portinari 2003) and provides the favoured solution to the "G dwarf problem" (e.g. Lynden-Bell 1975; Tinsley 1980; Chiosi 1980; Pagel 1989; Matteucci 1991) as shown in Figure 4.5.

The Galactic disk is divided into concentric cylindrical shells, which evolve independently; radial flows of gas (Portinari & Chiosi 2000) are neglected in the present work.

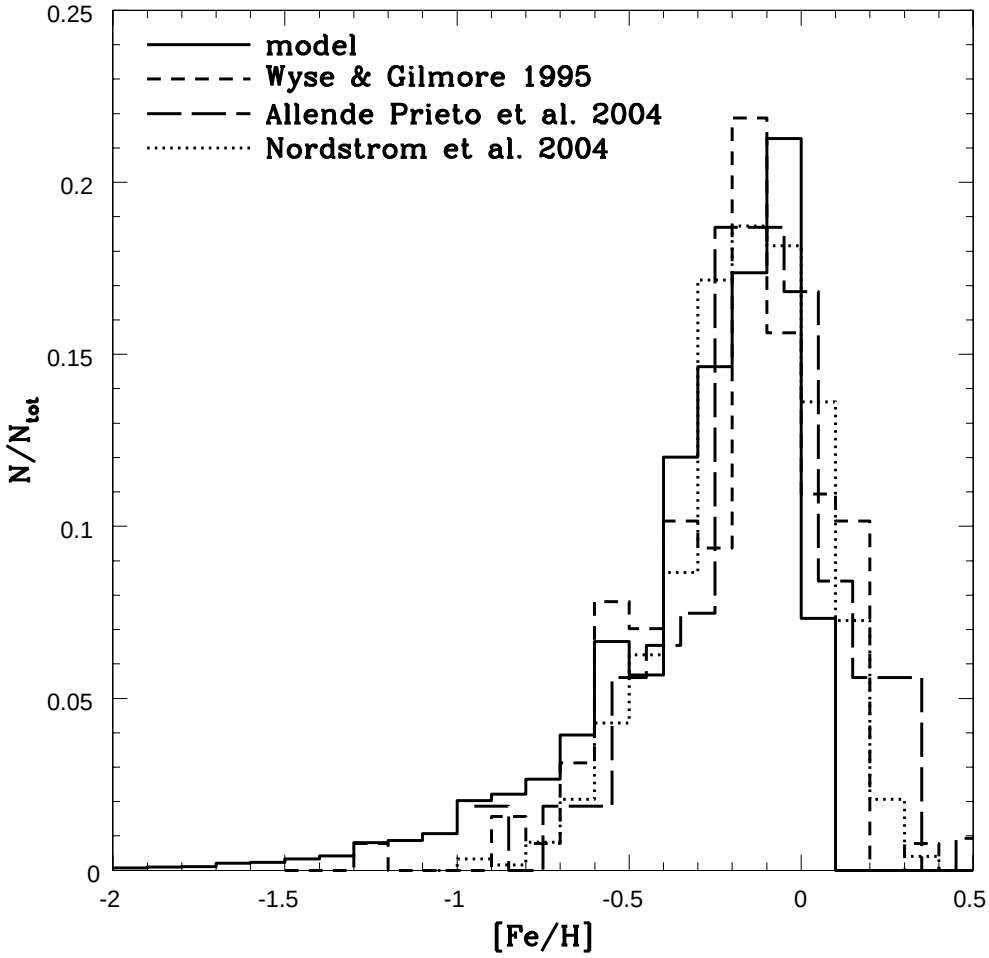

Figure 4.5: *Observational data on the local metallicity distribution, in relative number, of long–lived stars shown together with the prediction of our open model A (see Section 4.4 for further details).*

Each ring consists of a homogeneous mixture of gas and stars, so that for each ring the only independent variable is the time t ("one zone" model, Talbot & Arnett 1971). Galactic discs are comfortably described in terms of surface mass density $\sigma(r, t)$, which depends both on the galactocentric radius r of the ring and also on time t, since in each ring the surface density is growing in time due to gradual infall of gas. Since we apply the model only to the Solar Neighbourhood, in the following we drop the dependence on r.

If we indicate with $\sigma_g(t)$ the surface gas density, the gas fraction in the ring at any given time t is the ratio

$$\frac{\sigma_g(t)}{\sigma(t)} \tag{4.1}$$

while the stellar surface density is

$$\sigma_s(t) = \sigma(t) - \sigma_g(t). \tag{4.2}$$

In closed models the total surface density $\sigma(t)$ is constant and the other quantities can be normalized with respect to it. In open models it is suitable to normalize with respect to the total surface density at the present age of the Galaxy t_G i.e. at the final stage of the model. It is therefore convenient to introduce the normalized surface gas density

$$G(t) = \frac{\sigma_g(t)}{\sigma(t_G)}. \tag{4.3}$$

In each ring the gas is assumed to be chemically homogeneous, and the normalized gas density for each chemical species i is

$$G_i(t) = X_i(t)G(t) \tag{4.4}$$

where X_i is the fractionary mass abundance of species i and $\sum_i X_i = 1$, by definition. The chemical evolution of the ISM is the evolution of the set of the G_i's described by

$$\frac{d}{dt}G_i(t) = -X_i(t)\psi(t) + \int_{M_l}^{M_u} \psi(t-\tau_M)R_{M_i}(t-\tau_M)\phi(M)dM + \left[\frac{d}{dt}G_i(t)\right]_{inf} \tag{4.5}$$

where $\psi(t)$ is the SFR, $\phi(M)$ is the IMF, $R_{M_i}(t)$ is the mass fraction of a star of mass M ejected into the ISM in the form of element i, M_l and M_u are the lower and upper limit for stellar mass respectively and τ_M is the lifetime of a star of mass M. The first term on the right hand side represents the depletion of species i from the ISM due to star formation; the second term represents the amount of species i returned to the ISM by stellar ejecta and the third term is the contribution of the infalling gas. The main ingredients are described in more details in the following subsections.

4.3.1 Stellar ejecta

To solve equation (4.5) one needs to calculate

$$R_{M_i}(t) = \frac{E_{M_i}(t)}{M} \tag{4.6}$$

where $E_{M_t}(t)$ is the amount (in $M_\odot$) of species i which the star expels into the surrounding environment via stellar wind, supernova explosion or planetary nebula. The stellar ejecta $E_{M_i}(t)$, or rather $E_{M_i}(t, Z)$ since metallicity dependence is also taken into

account are also taken from Portinari et al. (1998) and Marigo (2001). The restitution fractions depend therefore on metallicity as well.

To follow the temporal behaviour of different chemical species, the *instantaneous recycling approximation* is dropped by taking into account the role of finite lifetimes for stars of different masses. Stellar lifetimes are adopted from the same Padova tracks which served as the base for the adopted stellar yields and therefore allow to consider the effects of different metal content not only on the ejecta but also on the lifetimes. The lifetimes are calculated as the sum of the H-burning and He-burning timescales.

Each star is assumed to expel its ejecta all at once at the end of its lifetime and that the ejected material is immediately mixed in the ISM, which remains always homogeneous. This *instantaneous mixing approximation* is suitable to reproduce the average trends of abundances observed in the disc, while it cannot model the observed scatter of the data around the average trend.

Notice that the ejecta of a given star are the sum of its yields plus the original material which is returned to the ISM without being processed. The effect of stellar ejecta is thus of fundamental importance in the chemical evolution model, but as long as we are interested in a differential quantity such as $\Delta Y/\Delta Z$ the stellar yields only provide a valuable insight, as we have already discussed in Section 4.2.

4.3.2 The infall term

In open models the surface mass density $\sigma(t)$ increases by slowly accreting gas at a rate $\dot{\sigma}_{inf}(t)$ until it reaches the observed present value. An infall rate exponentially decreasing in time with a timescale τ

$$\dot{\sigma}_{inf}(t) = A\, e^{-\frac{t}{\tau}} \tag{4.7}$$

well reproduces the results of dynamical models (e.g. Larson 1976; Carraro et al. 1998; Sommer–Larsen et al. 2003). A is obtained by integrating over time and by requiring that at the age t_G the observed present surface mass density $\sigma(t_G)$ is matched

$$A\left(1 - e^{-\frac{t_G}{\tau}}\right)\tau = \sigma(t_G). \tag{4.8}$$

The contribution of the infalling gas to the evolution of the gas fraction $G(t)$ is

$$\left[\frac{d}{dt}\,G(t)\right]_{inf} = \frac{\dot{\sigma}_{inf}(t)}{\sigma(t_G)} \tag{4.9}$$

and for each single chemical species i

$$\left[\frac{d}{dt}\,G_i(t)\right]_{inf} = \frac{\dot{\sigma}_{inf}(t)X_{i,inf}}{\sigma(t_G)} \tag{4.10}$$

which gives the third term on the right hand side of Eq. (4.5).

4.3.3 The star formation rate

The formulation for the SFR introduced by Talbot & Arnett (1975) is adopted

$$\frac{d}{dt}\,\sigma_g(r,t) = -\nu \left[\frac{\sigma(r,t)\sigma_g(r,t)}{\sigma^2(r_\odot,t_G)}\right]^{\kappa-1} \sigma_g(r,t). \tag{4.11}$$

Here, κ (usually ranging from 1 to 2) is the exponent of the Schmidt (1959) law for star formation, $\psi \propto \rho^\kappa$; $\sigma(r_\odot,t_G)$ is the surface mass density at $(r_\odot,t_G)$, adopted as a normalization factor; ν is a free parameter for the star formation efficiency. The dependence on the surface mass density is introduced because the SFR is related to the local dynamical timescale, which is shorter where the mass density is larger.

In terms of the formalism introduced in the previous Sections, the adopted SFR becomes

$$\psi(r,t) = \nu \left[\frac{\sigma(r,t)\sigma(r,t_G)}{\sigma^2(r_\odot,t_G)}\right]^{\kappa-1} G^\kappa(r,t) \tag{4.12}$$

and limiting to the solar ring simplifies to

$$\psi(t) = \nu \left[\frac{\sigma(t)}{\sigma(t_G)}\right]^{\kappa-1} G^\kappa(t) \tag{4.13}$$

where the dependence on r has been dropped and ν is to be fixed so as to reproduce the features of the Solar Neighbourhood.

4.3.4 The initial mass function

The Kroupa (1998) IMF derived for field stars in the Solar Neighbourhood is adopted[1]

$$\phi(M)dM \propto M^{-\alpha}dM \tag{4.14}$$

where

$$\alpha = \begin{cases} 0.5 & M \leq 0.5 \\ 1.2 & 0.5 < M \leq 1.0 \\ 1.7 & 1 < M < 100 \end{cases}$$

This IMF is steeper than the Salpeter one ($\phi(M) \propto M^{-1.35}$) in the high mass range ($M > 1M_\odot$) but it flattens out progressively at low masses ($M < 1M_\odot$). The steep slope in the high mass range was actually taken after Scalo (1986). In a more recent determination Kroupa (2001) finds instead a shallower slope of 1.3, close to the Salpeter value, but the steeper Scalo slope is recovered if unresolved binary systems are taken into account (Kroupa 2002). Also, steeper slopes are favoured in the average field with respect to individual star clusters (Kroupa & Weidner 2003).

The adopted IMF is one of the ingredients which compose a GCE model, and we have already shown in Section 4.2 that the choice between different types of IMF has little impact for the purpose of the present investigation.

[1] We adopt an upper mass cutoff of $100\ M_\odot$, i.e. no very massive stars are supposed to be present.

4.4 The evolution of helium

The model previously presented is used to study the chemical evolution of helium in the Solar Neighbourhood. Standard observational counterparts for chemical models such as the (1) current gas fraction, (2) the rate of type I and type II SNe, (3) the age–metallicity relation, (4) the past and current estimated SFR, (5) the metallicity distribution of long–lived stars (G dwarf problem) are used to calibrate the free parameters of the model.

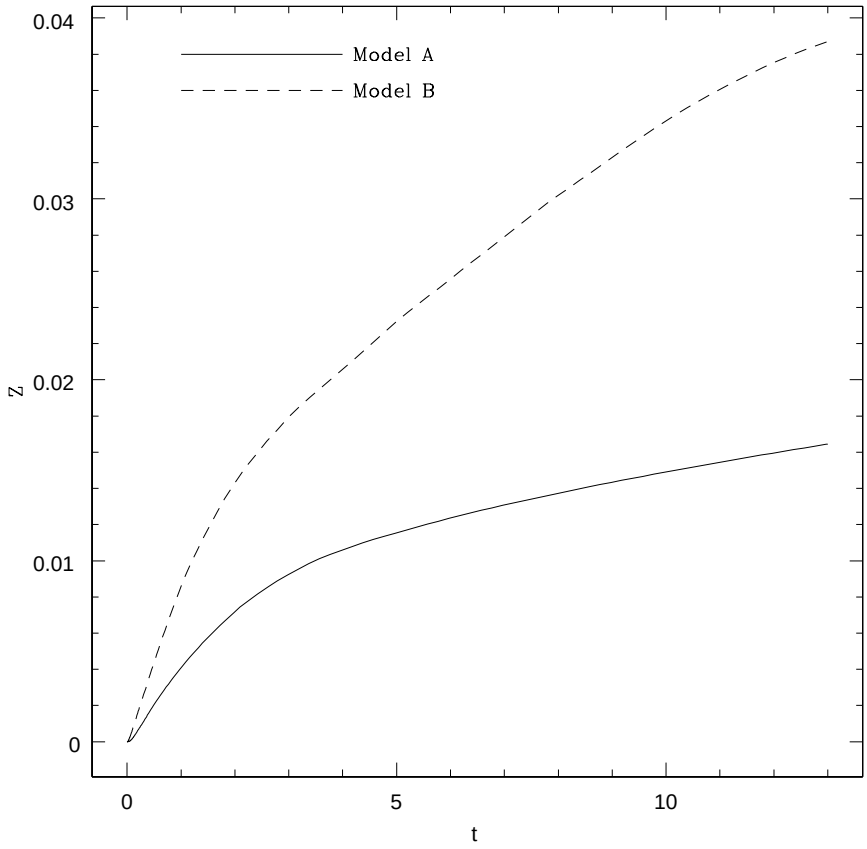

Figure 4.6: *Evolution of the metal mass fraction with time for the two models used to study the evolution of helium in the Solar Neighbourhood. Details on the two models are discussed in the text.*

In our case the free parameters are the star formation efficiency (ν), the exponent of the star formation law (κ), the infall timescale (τ) and the amplitude factor for the SNe Ia. The other parameters adopted in the model are directly constrained by observational

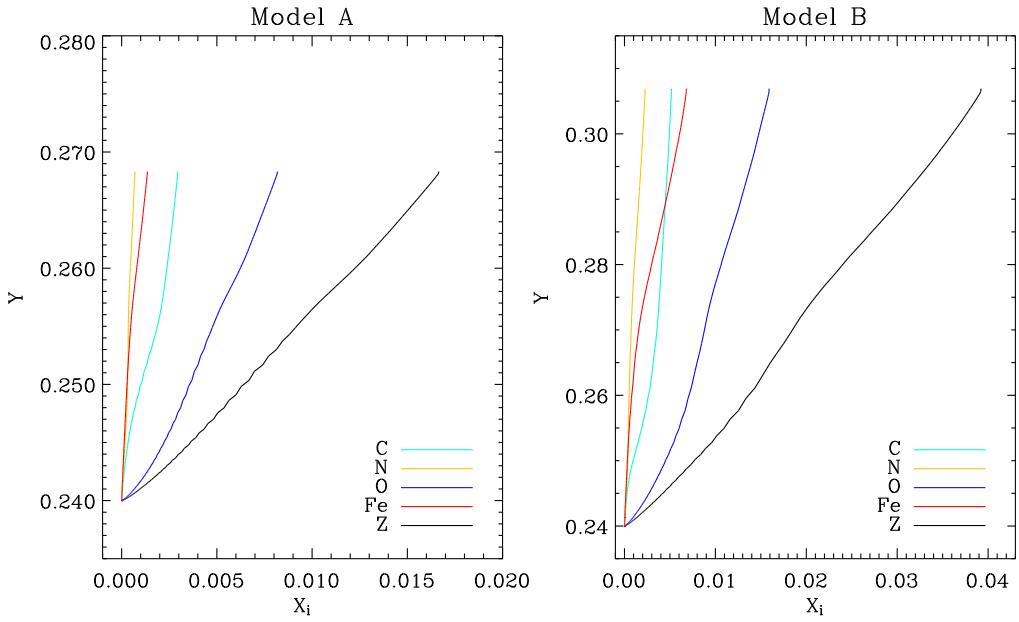

Figure 4.7: *The evolution of the helium mass fraction Y as function of the total metal mass fraction Z. Also shown is the evolution of Y as function of the mass fraction of carbon (*C*), oxygen (*O*), nitrogen (*N*) and iron (*Fe*).*

determinations: the local surface mass density for the Solar Neighbourhood is chosen to be $\sigma(r_\odot) = 50 M_\odot / \mathrm{pc}^2$ (Holmberg & Flynn 2000, 2004) and $t_G = 13$ Gyr, consistent with the WMAP value for the age of the Universe (Spergel et al. 2007). The infalling material is assumed to be protogalactic gas, with primordial chemical composition $X = 0.76$, $Y = 0.24$ and $Z = 0$ (see also Chapter 2). Notice that the value of Y_P does not influence the model predictions on the rate of helium vs. metals production by the stellar populations, $\Delta Y / \Delta Z$.

As we discuss in the following, the helium–to–metal enrichment ratio is actually quite insensitive to the exact calibration of the chemical evolution model, the reason being that $\Delta Y / \Delta Z$ mostly depends on the adopted stellar yields. The calibration of a model that satisfactorily matches all the constraints previously mentioned is not straightforward. We have selected two models for the chemical evolution of the Solar Neighbourhood. Model A is built to match the observational constraints previously mentioned whereas model B is built *ad hoc* to reach a high Z at the present time t_G (Figure 4.6) since our observational constraints in Paper II include highly metal–rich local stars (Casagrande et al. 2007). In fact model A is calibrated to match the average properties of the Solar Neighbourhood, and it does not reach a metal mass fraction higher than $Z_\odot \sim 0.017$, as the majority of local stars are of metallicity lower than the Sun (Figure

4.5). The difficulty is even more striking considering that such a $Z_{\odot}$ should have already been in place 4.6 Gyr ago. Interestingly, the low Z for the Solar Neighbourhood returned by our GCE model A is in better agreement with the abundances measured in the local ISM (e.g. André et al. 2003) as well as in nearby B stars (e.g. Gies & Lambert 1992; Cunha & Lambert 1992; Sofia & Meyer 2001) and it appears also consistent with the updated solar metallicity (Asplund et al. 2005).

The higher metal mass fraction in model B is obtained by adopting a very short infall timescale ($\tau = 2$ Gyr) which reduces the amount of pristine gas newly supplied to the Solar Neighbourhood, whereas increasing the efficiency of the SFR has minor impact. In order to reach a high metal mass fraction in the Solar Neighbourhood, a higher efficiency of the the SNe Ia is also assumed in model B. Although model B is not a realistic description of the chemical evolution of the Solar Neighbourhood, it is useful to demonstrate that the slope of $\Delta Y/\Delta Z$ is rather insensitive to the details of the chemical evolution model adopted. The theoretical predictions presented here are therefore robust.

Figure 4.7 shows the predicted evolution of the helium mass fraction Y as function of the total metal mass fraction Z and of the mass fraction of other single elements (C, N, O, Fe). When the relation of Y vs. Z is considered, such a plot can be regarded as the theoretical counterpart of the extensive observational work of Paper II and reproduced also in Figure 3.2 where we measured Y and Z from nearby K dwarf stars. The helium–to–metal enrichment ratio predicted by both chemical evolution models (A and B) is well approximated by a linear relationship, although that is not necessarily the case when the abundances of single elements are considered. In both models the slope over the entire Z range is $\Delta Y/\Delta Y = 1.7$. A discussion of the slope in the very metal–poor regime has already been done in Chapter 2, and it is very close to the results found here. The helium–to–metal enrichment ratio predicted by our chemical evolution models also agrees with the slope found in Paper II using nearby K dwarfs with metallicity around and above solar.

For subsolar metallicities, the $\Delta Y/\Delta Z$ found using K dwarfs is considerably different from the theoretical expectation discussed in this Section. At the same time, the good agreement between the theoretical and the empirical $\Delta Y/\Delta Z$ measured above solar metallicity and the theoretical and the empirical $\Delta Y/\Delta(\mathrm{O/H})$ in low metallicity HII regions ensures that it is possible to use the GCE model presented in this Chapter to obtain meaningful conclusions on the cosmic evolution of helium.

We have already clearly stated that we believe the low helium abundances found in Paper II stem from inadequacies in the extant stellar models for low mass stars. Nonetheless, for the sake of completeness, we briefly discuss what this result would imply taken at face value. In Figure 3.2 the mean slope $\Delta Y/\Delta Z = 9.2$ below $Z = 0.013$ would extrapolate to a primordial helium mass fraction $Y_P = 0.13$. From the discussion in Chapter 2 is obvious that there is overwhelming evidence for a much higher $Y_P \sim 0.24$ so that we do not question the BBN constraint here. The main problem is to find a suitable astrophysical mechanism responsible for such a large depletion/destruction of

helium (of order $\Delta Y \sim 0.10$) in metal–poor star forming regions of the Galaxy. Besides, it would still be challenging for any GCE model to produce a helium enrichment rate capable to fully counterbalance the depletion/destruction previously mentioned.

It is interesting to notice that similar, or even larger ΔY are obtained when theoretical stellar isochrones are used to fit the stellar populations in some globular clusters, like ω Centauri (Norris 2004) or NGC2808 (D'Antona et al. 2005). In such cases, the helium abundance for the most metal–poor population is chosen to be primordial $Y_P \sim 0.24$, thus implying $Y \sim 0.35 - 0.40$ for the other populations observed in the clusters. Nonetheless, from the study of the nearby K dwarfs we have found that in the metal–poor regime, the observed main-sequence is considerably narrower than predicted by models with standard $\Delta Y/\Delta Z \sim 2$. The only solution to fit the observations with present models is to assume a much steeper slope for the helium–to–metal enrichment ratio below, say, $Z = 0.013$. We strongly suspect that the result obtained for the K dwarfs stems from inaccuracies in the current metal–poor low mass stellar models and it would be interesting to check weather the extreme values of $\Delta Y/\Delta Z$ deduced by isochrone fitting the main-sequence of some globular clusters are at least partly the same problem. The inverted blue and red main-sequence in ω Centauri would still imply a considerable helium enrichment, but maybe not so high as it is currently believed ($\Delta Y/\Delta Z \sim 70$ Piotto et al. 2005) and very challenging to explain (e.g. Karakas et al. 2006; Choi & Yi 2008).

CHAPTER 5
Summary of the original publications

> "Success is not final, failure is not fatal: it is the courage to continue that counts"
>
> Winston Churchill

This thesis consists of three journal papers. The main goals, methods and results of each are summarized below. After the summaries, I briefly present prospects for immediate research arising from the work.

- **Paper I**: Casagrande L., Portinari L., Flynn C., "Accurate fundamental parameters for lower main-sequence stars", 2006, MNRAS, 373, 13-44
- **Paper II**: Casagrande L., Flynn C., Portinari L., Girardi L., Jimenez R., "The helium abundance and $\Delta Y/\Delta Z$ in lower main-sequence stars", 2007, MNRAS, 382, 1516-1540
- **Paper III**: Casagrande L., Flynn C., Bessell M., Koen C., "M dwarfs: effective temperatures, radii and metallicities", submitted to MNRAS, 25 pages

The author's contribution:

The author performed some of the optical observations presented in Paper I using the remotely operated KVA telescope in LaPalma. Significant help in using the reduction software for the photometric observations came from C. Flynn. The development of the InfraRed Flux Method (Paper I) and of the Multiple Optical Infrared TEchnique (Paper III) was done by the author as well as most of the analysis and the writing of all three papers. The near–infrared observations are all from 2MASS. The theoretical stellar models used in Paper II were provided by L. Girardi and R. Jimenez. Most of the optical observations presented in Paper III were conducted by C. Koen and for the same paper M. Bessell provided significant help in discussing the results. L. Portinari and C. Flynn provided fundamental support for the chemical evolution model of the Solar Neighbourhood discussed in Chapter 2 – 4.

5.0.1 Paper I

As discussed throughout the thesis, low mass stars can be seen as fossils of the Galaxy's evolution. Their accurate characterization, both observationally and theoretically, is of fundamental importance for unveiling the formation and evolution of the Milky Way. To successfully achieve such a task accurate fundamental physical parameters and thoroughly tested theoretical stellar models are needed.

This paper presents accurate $BV(RI)_C JHK_S$ photometry for a large sample of nearby G and K dwarfs. The comparison between the observed and synthetic colours has been used to test the most recent theoretical model atmospheres (ATLAS9 and MARCS) for these stars. Such a comparison shows a generally good agreement. Special attention has been paid to the accuracy and homogeneity in generating synthetic colours, with a special care in discussing the effect of the adopted zero–points and absolute calibration. The latter point is also crucial for setting the scale of stellar effective temperatures determined via the IRFM.

The IRFM (Blackwell & Shallis 1977; Blackwell, Shallis & Selby 1979; Blackwell, Petford & Shallis 1980) is known to be one of the most reliable techniques to derive fundamental stellar parameters i.e. effective temperatures, bolometric luminosities and angular diameters. It uses infrared photometry as a sensitive proxy of the stellar effective temperature and a great deal of observational information to make the derivation of the stellar parameters almost model independent. In this paper, an implementation of the IRFM has been done *ab initio*, so as to keep full control on all possible sources of uncertainties, in particular because we put these stars to work in Paper II, using them to track helium production in the Galaxy. Major improvements with respects to similar work done in the past are the excellent quality and homogeneity of the observational data (also thanks to a large near–infrared survey as 2MASS), the use of multi–band photometry covering the wavelength range where these stars emit most of their flux ($\sim 0.4 - 2.2\,\mu\mathrm{m}$) in order to recover their bolometric luminosity, the adoption of the latest generation of model atmospheres and the most recent zero–points and absolute calibration for Vega as thoroughly discussed in Appendix A of the paper.

The tightness of the derived colour–temperature, colour–angular diameter and colour–luminosity relations reflects the high quality of the input data used and the internal accuracy of the work. Because of the adopted 2MASS absolute calibration, the proposed temperature scale is found to be about $100\,\mathrm{K}$ hotter than recent analogous determinations in literature, but in very good agreement with various spectroscopic temperature scales. We thus conclude that T_{eff} determinations for lower main-sequence stars still retain systematics of the order of a few percent. Currently, interferometric measurements of G and K dwarf angular diameters break only partly this impasse on the temperature scale. In fact, angular diameters measured via interferometry must be corrected for limb-darkening, thus introducing model dependence. With respect to classical 1D model atmospheres, 3D models predict different limb-darkening coefficients, which imply smaller angular diameters and thus hotter effective temperatures (Allende Prieto et

al. 2002). The departure from 1D to 3D limb-darkening is more relevant for hotter stars and decreases considerably going to cooler M dwarfs (Bigot et al. 2006), as discussed also in Paper III.

5.0.2 Paper II

In this article the fundamental stellar parameters determined in Paper I are used to test some of the most up–to–date stellar models, newly computed for various metallicities and helium abundances. The aim is to measure the helium–to–metal enrichment ratio $\Delta Y/\Delta Z$, a diagnostic of the chemical history of the Solar Neighbourhood as discussed in Chapter 4.

Taking advantage of the detailed analysis performed in Paper I, we have performed a direct comparison between stellar models and observations in the $M_{\rm Bol} - T_{\rm eff}$ plane, thus working directly with physical quantities. For the parameter space covered by the isochrones, the number of stars used, the accuracy and homogeneity of the data —crucial when it comes to analysing small differential effects in the HR diagram— the analysis performed in Paper II is the most stringent test on the helium content of lower main-sequence stars undertaken to date.

Around and above the solar metallicity the helium content scales with the metal mass fraction more or less consistently with GCE model prediction (Chapter 4), with $\Delta Y/\Delta Z \sim 2 \pm 1$ which is also the value usually assumed in the literature by a number of studies. Such a trend breaks down going to the lowest metallicities, where the broadening of the observed lower main-sequence is considerably narrower than predicted by theoretical stellar models under the standard assumption $\Delta Y/\Delta Z \sim 2$. To fit the position of metal–poor stars in the HR diagram, anomalously low helium abundances, well below the standard BBN predictions, must be used. Possible alternatives to such low helium abundances are discussed throughout the paper. Including diffusion in stellar models and accounting for non-LTE effects in deriving metallicities do not go very far to solve the problem. A viable option is to assume a mixing–length that decreases steadily with decreasing metallicity.

5.0.3 Paper III

Paper III extends the results of Paper I to M dwarfs. Although M dwarfs make up about half of the stellar mass of the Galaxy, until now discussions on these objects could just be largely qualitative because of the intrinsic difficulties in determining their stellar parameters. Major recent improvements in determining abundances for M dwarfs, in their theoretical model atmospheres and the availability of very accurate and homogeneous photometry for them, make it very timely to extend to M dwarfs the work started in Paper I.

A new technique, the Multiple Optical Infrared TEchnique (MOITE) is introduced. The MOITE exploits the bolometric to monochromatic flux ratios in different bands

(rather than in the infrared only, as the IRFM does) to recover the fundamental stellar parameters for M dwarfs. A strong sensitivity to the metallicity has been found for the bolometric to monochromatic flux ratios of cool dwarfs. By exploiting such a features, the MOITE provides a tool to determine photometrically the metal content in dwarfs of late spectral type.

The results provided by the MOITE offer thus the interesting opportunity of effectively using M dwarfs as tracers of the Galactic Chemical Evolution. The results obtained in this paper also have important consequences for the study and modelling of low mass stars. A comparison with the widely used low mass stellar models of Baraffe et al. (1998) is made. Thanks to the accuracy and homogeneity of the data, a sharp transition between K and M dwarfs has been found. Such a feature is not yet reproduced by stellar models and appears to be related to a sudden increase in the radii of M dwarfs. This discrepancy between the observed and the theoretical radii for M dwarfs is discussed in the light of similar results obtained in recent years from much smaller samples of M dwarfs.

5.0.4 Future prospects

The technique developed in Paper I and III well suits to be applied to other classes of stars, so as to cover a wider temperature and metallicity range. A better definition of the effective temperature scale, eventually extending to the extremely metal–poor regime would be of importance for a variety of studies, from Galactic archaeology to stellar modelling.

Uncertainties in the Vega zero points and absolute calibration still hinder much of a progress in reducing the systematic errors that plague the temperature scale. More angular diameters measurements, corrected using limb-darkening coefficients computed from 3D model atmospheres would greatly help to firmly establish the temperature scale in different regions of the HR diagram, finally solving *"il dilemma delle calibrazioni astrofisiche"* (Gustafsson & Gråe-Jørgensen 1985). VLTI angular diameter measurements for three solar type stars will be soon available as Co-I in the VLTI accepted proposal 081.D-0412.

The technique presented in Paper III for determining the metallicity of M dwarfs needs to be further tested. New photometric and spectroscopic observations of more *Hipparcos* common proper–motion companions with M dwarf secondaries from the list of Gould & Chanamé (2004) are a simple way forward as metallicities for the M dwarfs can be deduced from the binary hosts. We could obtain ten times more stars than analysed in Paper III.

The IRFM and the MOITE are unique tools for extracting stellar parameters and I will continue updating them to be valuable for the latest data, most notably upcoming photometric surveys such as SkyMapper (Keller et al. 2007). With Mike Bessell, we are obtaining optical spectrophotometry for few hundreds of stars whose fundamental parameters have already been determined with the IRFM/MOITE. The data will be

similar to those expected from the low-resolution spectrograph on *GAIA*. The precise IRFM/MOITE–based data on nearby stars will be used as a template onto which calibrate new tools for extracting reliable stellar parameters from such low-resolution spectra, so as to readily identify the best targets for further follow-up observations.

GAIA, as well as other ground based projects such as *RAVE*, *SEGUE* and *0Z* will produce a vast amount of data for a billion halo, disc, and bulge stars. Reconstructing the formation and evolution of the Milky Way in a star–by–star fashion will be a crucial step towards achieving a successful theory of Galaxy formation. Such data will also considerably improve our understanding of Galactic Chemical Evolution.

The further use of the chemical evolution model presented in Chapter 4 will be very valuable for studying the evolution of the helium and other elements in the Solar Neighbourhood. It will be challenging to try to use such approach to independently confirm the recent update in the solar chemical composition (Asplund et al. 2005).

As a result of such new abundances, the solar model is currently under profound revision. The results provided by Paper II also suggest that theoretical stellar models for metal–poor low mass stars need to be improved, possibly accounting for a metallicity dependent mixing–length. Currently, 3D hydrodynamical models by treating convection in a fully self-consistent way offer the best option to test any dependence of the mixing–length with metallicity. Expanding the range within which we will confidently use stellar models will also push forward the limit of our knowledge on the formation and evolution of the Galaxy.

Bibliography

Allende Prieto C., Asplund M., López R.J.G., Lambert D.L., 2002, ApJ, 567, 544

Allende Prieto C., Barklem P.S., Lambert D.L., Cunha K., 2004, 420, 183

Alonso A., Arribas S., Martínez-Roger C., 1996, A&A, 117, 227

Alpher R.A., Bethe H.A., Gamow G., 1948, Phys. Rev., 73, 803

André et al., 2003, ApJ, 591, 1000

Asplund M., Grevesse N., Sauval A.J., 2005, ASPC, 336, 25

Asplund M., Lambert D.L., Nissen P.E., Primas F., Smith V.V., 2006, ApJ, 644, 229

Bahcall J.N. Serenelli A.M., Basu S., 2006, ApJS, 165, 400

Balser D.S., 2006, AJ, 132, 2326

Bania T.M., Rood R.T., Balser D.S., 2002, Nat, 415, 54

Baraffe I., Chabrier G., Allard F., Hauschildt P.H., 1998, A&A, 337, 403

Basu S., Antia H.M., 2008, Phys. Rep., 457, 217

Basu S., Pinsonneault M.H., Bahcall J.N., 2000, ApJ, 529, 1084

Bensby T., Feltzing S., Lundström I., 2003, A&A, 410, 527

Bigot L., Kervella P., Thévenin F., Ségransan D., 2006, A&A, 446, 635

Blackwell D.E., Shallis M.J., 1977, MNRAS, 180, 177

Blackwell D.E., Shallis M.J., Selby M.J., 1979, MNRAS, 188, 847

Blackwell D.E., Petford A.D., Shallis M.J., 1980, A&A, 82, 249

Bonfils X., Delfosse X., Udry S., Santos N.C., Forveille T., Ségransan D., 2005, A&A, 442, 635

Bonifacio P., Molaro P., 1997, MNRAS, 285, 847

Bonifacio P. et al., 2007, A&A, 462, 851

Brewer M.M., Carney B.W., 2006, AJ, 131, 431

Brown J.A., Sneden C., Lambert D.L., Dutchover E.J., 1989, ApJS, 71, 293

Burbidge E.M., Burbidge G.R., Fowler W.A., Hoyle F., 1957, RvMP, 29, 547

Burles S., Tytler D., 1998, ApJ, 499, 699

Carigi L., Peimbert M., 2008, astro-ph/0801.2867

Carollo D. et al., 2007, Nat, 450, 1020

Carraro G., Lia C., Chiosi C., 1998, MNRAS, 297, 1021

Casagrande L., Portinari L., Flynn C., 2006, MNRAS, 373, 13

Casagrande L., Flynn C., Portinari L., Girardi L., Jimenez R., 2007, MNRAS, 382, 1516

Casagrande L., Flynn C., Bessell M., Koen C., 2008, MNRAS, submitted

Casagrande L., 2008, Annales Universitatis Turkuensis, "The Cosmic Production of Helium" alias "He researched ^{4}He four (light) years", or "Why research ^{4}He four (light) years?"

Castellani V., degl'Innocenti S., Marconi M., 1999, A&A, 349, 834

Chiappini C., Renda A., Matteucci F., 2002, A&A, 395, 789

Chiosi C., 1980, A&A, 83, 206

Chiosi C., 2007, ASPC, 374, 439

Chiosi C., Matteucci F., 1982, A&A, 105, 140

Chiosi C., Bertelli G., Bressan A., 1992, ARA&A, 30, 235

Choi E., Yi S.K., 2008, astro-ph/0804.1598

Christensen-Dalsgaard J., Proffitt C.R., Thompson M.J., 1993, ApJ, 403, 75

Conrath B.J., Gautier D., 2000, Icar, 144, 124

Cox J.P., Giuli R.T., 1968, Principles of Stellar Structure. Gordon & Breach, New York

Cunha K., Lambert D.L., 1992, ApJ, 399, 586

D'Antona F., Bellazzini M., Caloi V., Pecci F.F., Galleti S., Rood R.T., 2005, ApJ, 631, 868

de la Reza R., 2000, IAU Symp., 198, 310

Dicke R.H., Peebles P.J.E., Roll P.G., Wilkinson D.T., 1965, ApJ, 142, 414

Edvardsson B., Andersen J., Gustafsson B., Lambert D.L., Nissen P.E., Tomkin J., 1993, A&A, 275, 101

Eggen O.J., Lynden-Bell D., Sandage A.R., 1962, ApJ, 136, 748

Eldridge J.J., Tout C.A., 2004, MNRAS, 353, 87

Faulkner J., 1967, ApJ, 147, 617

Feltzing S., Gustafsson B., 1998, A&AS, 129, 237

Feltzing S., Holmberg J., Hurley J.R., 2001, A&A, 377, 911

Fernandes J., Lebreton Y., Baglin A., 1996, A&A, 311, 127

Flynn C., Morell O., 1997, MNRAS, 286, 617

Freeman K., Bland-Hawthorn J., 2002, ARA&A, 40, 487

Fukugita M., Kawasaki M., 2006, ApJ, 646, 691

Gamow G., 1946, Phys. Rev., 70, 527

Gies D.R., Lambert D.L., 1992, ApJ, 387, 673

Gould A., Chanamé J., 2004, ApJS, 150, 455

Grevesse N., Sauval A.J., 1998, Space Sci. Rev., 85, 161

Gruenwald R., Steigman G., Viegas S.M., 2002, ApJ, 567, 931

Gustafsson B., Gråe-Jørgensen, 1985, IAU Symp., 111, 303

Hirschi R., Meynet G., Maeder A., 2005, A&A, 433, 1013

Holmberg J., Flynn C., 2000, MNRAS, 313, 209

Holmberg J., Flynn C., 2004, MNRAS, 352, 440

Iocco F., Mangano G., Miele G., Pisanti O., Serpico P.D., 2007, PhRvD, 75, 7304

Izotov Y.L., Thuan T.X., 2004, ApJ, 602, 2000

Izotov Y.I., Thuan T.X., Stasińska G., 2007, ApJ, 662, 15

Izotov Y.I., Chaffee F.H., Foltz C.B., Green R.F., Guseva N.G., Thuan T.X., 1999, ApJ, 527, 757

Jimenez R., Flynn C., MacDonald J., Gibson B.K., 2003, Sci, 299, 1552

Karakas A., Lattanzio J.C., 2007, PASA, 24, 103

Karakas A., Fenner Y., Sills A., Campbell S.W., Lattanzio J.C., 2006, ApJ, 652, 1240

Kawano L., 1992, NASA STI/Recon Technical Report N, 92, 25163

Keller S.C. et al., 2007, PASA, 24, 1

Kneller J.P., Steigman G., 2004, New Journal of Physics, 6, 117

Kolb E.W., Turner M.S., 1990, The early universe. Addison-Wesley, Frontiers in Physics, 69, Redwood City, USA

Korn A.J., Grundahl F., Richard O., Barklem P.S., Mashonkina L., Collet R., Piskunov N., Gustafsson B., 2006, Nat, 442, 657

Korn A.J., Grundahl F., Richard O., Mashonkina L., Barklem P.S., Collet R., Gustafsson B., Piskunov N., 2007, ApJ, 671, 402

Kotoneva E., Flynn C., Chiappini C., Matteucci F., 2002, MNRAS, 336, 879

Kroupa P., 1998, ASPC, 134, 483

Kroupa P., 2001, MNRAS, 322, 231

Kroupa P., 2002, Sci, 295, 82

Kroupa P., Weidner C., 2003, ApJ, 598, 1076

Larson R.B., 1974, MNRAS, 166, 585

Larson R.B., 1976, MNRAS, 176, 31

Levshakov S.A., Kegel W.H., Takahara F., 1998, ApJ, 499, 1

Luridiana V., Peimbert A., Peimbert M., Cerviño M., 2003, ApJ, 592, 846

Lynden-Bell D., 1975, Vistas in Astr., 19, 229

Maeder A., Meynet G., 1989, A&A, 210, 155

Maeder A., Meynet G., 2006, A&A, 448, 37

Meynet G., Maeder A., 2002, A&A, 390, 561

Meynet G., Ekström S., Maeder A., 2006, A&A, 447, 623

Marigo P., 2001, A&A, 370, 194

Marigo P., Girardi L., 2007, A&A, 469, 239

Matteucci F., 1991, ASPC, 20, 539

Matteucci F., 2001, The chemical evolution of the Galaxy, Astrophysics and space science library, Dordrecht: Kluwer Academic Publishers

Matteucci F., Greggio L., 1986, A&A, 154, 279

McWilliam A., 1997, ARA&A, 35, 503

Meléndez J., Ramírez I., 2004, ApJ, 615, 33

Nordström B. et al., 2004, A&A, 418, 989

Norris J.E., 2004, ApJ, 612, 25

O'Meara J.M., Tytler D., Kirkman D., Suzuki N., Prochaska J.X., Lubin D., Wolfe A.M., 2001, ApJ, 552, 718

O'Meara J.M., Burles S., Prochaska J.X., Prochter G.E., Bernstein R.A., Burgess K.M., 2006, ApJ, 649, 61

Olive K.A., Skillman E.D., 2004, ApJ, 617, 29

Olive K.A., Skillman E.D., Steigman G., 1997, ApJ, 483, 788

Pagel B.E.J., 1989, in Evolutionary phenomena in galaxies, Beckman J.E., Pagel B.E.J. eds., Cambridge University Press

Pagel B.E.J., 1997, Nucleosynthesis and Chemical Evolution of Galaxies, Cambridge University Press, Cambridge, UK

Pagel B.E.J., Patchett B.E., 1975, MNRAS, 172, 13

Pagel B.E.J., Portinari L., 1998, MNRAS, 298, 747

Pagel B.E.J., Simonson E.A., Terlevich R.J., Edmunds M.G., 1992, MNRAS, 255, 325

Peimbert M., Torres-Peimbert S., 1974, ApJ, 193, 327

Peimbert M., Torres-Peimbert S., 1976, ApJ, 203, 581

Peimbert A., Peimbert M., Luridiana V., 2002, ApJ, 565, 668

Peimbert M., Luridiana V., Peimbert A., 2007, ApJ, 666, 636

Penzias A.A., Wilson R.W., 1965, ApJ, 142, 419

Pettini M., 2006, ASPC, 348, 19

Pettini M., Bowen D.V., 2001, ApJ, 560, 41

Pinsonneault M.H., Walker T.P., Steigman G., Naranyanan V.K., 1999, ApJ, 527, 180

Piotto G. et al., 2005, ApJ, 621, 777

Portinari L., Chiosi C., 2000, A&A, 355, 929

Portinari L., Chiosi C., Bressan A., 1998, A&A, 334, 505

Pottasch S.R., Bernard-Salas J., Roellig T.L., 2007, A&A, 471, 865

Ritossa C., Garcia-Berro E., Iben I.J., 1996, ApJ, 460, 489

Romano D., Tosi M., Matteucci F., Chiappini C., 2003, MNRAS, 346, 295

Rood R.T., Bania T.M., Balser D.S., Wilson T.L., 1998, Space Sci. Rev., 84, 185

Ryan S.G., Norris J.E., Beers T.C., 1999, ApJ, 523, 654

Salpeter E.E., 1955, ApJ, 121, 161

Scalo J.M., 1986, Fund. Cosmic Phys., 11, 1

Schmidt M., 1959, ApJ, 129, 243

Searle L., Zinn R., 1978, ApJ, 225, 357

Smith M.S., Kawano L.H., Malaney R.A., 1993, ApJS, 85, 219

Sneden C., Lambert D.L., Whitaker R.W., 1979, ApJ, 234, 964

Sofia U.J., Meyer D.M., 2001, ApJ, 554, 221

Sommer-Larsen J., Götz M., Portinari L., 2003, ApJ, 596, 47

Songaila A., Wampler E.J., Cowie L.L., 1997, Nat, 385, 137

Spergel D.N. et al., 2003, ApJS, 148, 175

Spergel D.N. et al., 2007, ApJS, 170, 377

Spite F., Spite M., 1982, A&A, 115, 357

Steigman G., 1994, MNRAS, 269, 53

Steigman G., 2007, Annual Review of Nuclear and Particle Systems, 57, 463

Strömgren B., Gustafsson B., Olsen E.H., 1982, PASP, 94, 5

Suzuki T.K., Yoshii Y., Beers T.C., 2000, ApJ, 540, 99

Talbot R.J.J., Arnett W.D., 1971, ApJ, 170, 409

Talbot R.J.J., Arnett W.D., 1975, ApJ, 197, 551

Tegmark M. et al., 2004, PhRvD, 69, 3501

Tinsley B.M., 1980, Fund. Cosmic Phys., 5, 287

Vauclair S., Charbonnel C., 1998, ApJ, 502, 372

Ventura P., D'Antona F., Mazzitelli I., 2002, A&A, 393, 215

Viegas S.M., Gruenwald R., Steigman G., 2000, ApJ, 531, 813

Wagoner R.V., 1973, ApJ, 179, 343

Wallerstein G., 1962, ApJS, 6, 407

White S.D.M., Rees M.J., 1978, MNRAS, 183, 341

Wyse R.F.G., Gilmore G., 1995, AJ, 110, 2771

Yao W.M. et al., 2006, J. Phys. G. Nucl. Part. Phys., 33, 1

Original papers